# Neutron Electric Dipole Moment Experiment

## A.1 Scientific Motivation

### A.1.a General Introduction

Precision measurements of the properties of the neutron present an opportunity to search for violations of fundamental symmetries and to make critical tests of the validity of the Standard Model (SM) of electroweak (EW) interactions. These experiments have been pursued with great energy and interest since Chadwick [i] discovered the neutron in 1932.

Searches for the electric dipole moment (EDM) of the neutron (nEDM) date back to a 1957 paper of Purcell and Ramsey [ii]. This paper led to an experiment using a magnetic-resonance technique at Oak Ridge National Laboratory (ORNL), where they established a value of $d_n = (-0.1 \pm 2.4) \times 10^{-20}$ $e$·cm [iii]. In the intervening 30 years, a series of measurements of increasing precision have culminated in the current best limit of $d_n < 3 \times 10^{-26}$ $e$·cm (90% C.L.) obtained in measurements at the Institute Laue-Langevin (ILL) reactor at Grenoble [iv].

The physics motivation for these measurements has been widely discussed. A search for a nonzero value of the nEDM is a search for a violation of time-reversal (*T)* invariance. To date, there is only one measurement (a comparison of neutral $K$ and $\overline{K}$ meson decay) in which $T$ violation has been seen directly [v]. The asymmetry in these rates is found to be $(6.6 \pm 1.3 \pm 1.0) \times 10^{-3}$ and is consistent with the SM.

The SM prediction for the nEDM is at the $10^{-31}$ $e$·cm level, below the reach of current measurements by six orders of magnitude [vi]. The only violation of the SM that has been observed is the recent measurements of the neutrino mass. There are many proposed models of the EW interaction that are extensions beyond the SM and that raise the predicted value of the nEDM by up to seven orders of magnitude. Some of these are already excluded by the current limit on the nEDM. The proposed experiment has the potential to reduce the acceptable range for predictions by two orders of magnitude and to provide a significant challenge to these extensions to the SM. Conversely, if a new source of $T$ violation is present in nature, that is relevant to this hadronic system, this experiment offers an intriguing opportunity to measure a nonzero value of the nEDM. Observation of a violation of $T$ invariance through measurement of the nEDM would be of fundamental significance.

This project invokes a new technique for searching for the EDM of the neutron which offers unprecedented sensitivity. It is based on the traditional magnetic-resonance technique in which the magnetic dipole moment of a neutron is placed in a plane perpendicular to parallel magnetic and electric field. The magnetic field is quite weak and the electric field is as strong as possible. The impact of the electric field on the precession of the neutron is characterized by the first moment of the neutron charge distribution, $d_n$, its EDM. All experiments to date have assigned a zero value to the nEDM. There has been an impressive reduction, with time, of the experimental limit for $d_n$ as illustrated in Fig I-1.

The nEDM provides a very sensitive test of the SM. A nEDM measurement, with two orders of magnitude improvement over the current experimental limits, presents an excellent opportunity to challenge the extensions beyond the SM and to search for new physics in nonstrange systems in the $T$ sector.

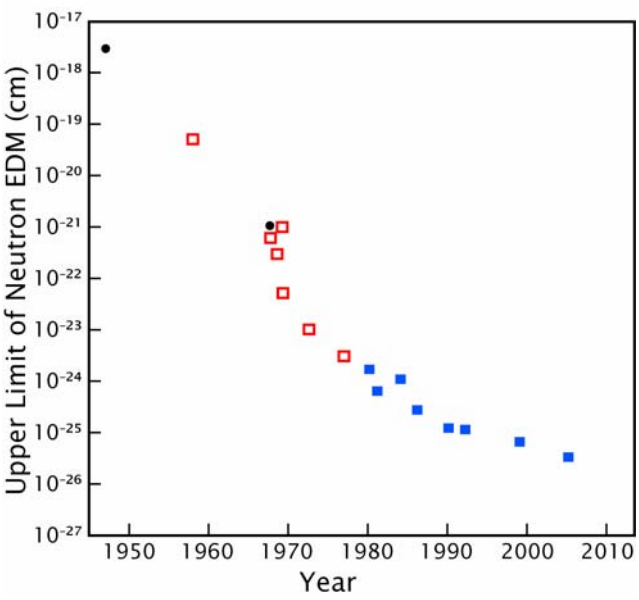


Fig. I-1.Upper limits of nEDM plotted as a function of year of publication. The solid circles correspond to neutron-scattering experiments. The open squares represent in-flight magnetic-resonance measurements, and the solid squares signify ultracold neutron (UCN) magnetic-resonance experiments.

**A.1.b. Theoretical Motivation**

The search for a nEDM, $d_n$, aims to discover new physics in the *CP* violating sector. A focus on *CP* violation is suggested by the critical importance which this symmetry has assumed in constructing theories of modern particle physics. More broadly, it acknowledges the importance of *CP* violation in shaping our understanding of the origins and evolution of the universe. In particular, explaining the origin of the baryonic matter of the universe is an important goal for nuclear physics [vii]. While the *CP* violation present in the SM suffices to explain what has been observed in the kaon and *B* meson systems, it is not sufficient to explain the small excess of baryons over antibaryons in the present universe. This new measurement of $d_n$—with its substantially greater sensitivity to new *CP* violation—provides a powerful tool in this quest.

The role of symmetry, including the observed breaking of the discrete symmetries of parity *P* and *CP*, has been particularly significant for the construction of the SM. Parity violation, which has been measured in many systems, is well represented in the SM through a definitive chiral *V-A* coupling of fermions to gauge bosons. The information available on *CP* violation, while much more limited, has had a profound impact. Indeed, the decay of neutral kaons anticipated the three-generation structure of the SM as we now know it.

Although the deeper reasons for the *P* and *CP* violation of the SM have yet to be understood, *CP* violation is arguably the more mysterious of the two. It occurs in two places within the model: as a complex phase in the Cabibbo-Kobayashi-Maskawa (CKM) matrix that characterizes charge changing weak interactions of quarks, and as total derivative in the $SU(3)_C$ Lagrangian that does not vanish because of the topology of the vacuum. The *CP* violation observed in the neutral kaon system and in the decays of *B* mesons is consistent with the presence of the phase factor. On the other hand, present limits on $d_n$ and the $^{199}$Hg EDM imply that the coefficient of the *CP* violating term in the strong Lagrangian is exceedingly small. In neither case does the strength of the associated *CP* violation allow us to explain the observed abundance of baryonic matter over antimatter. Thus, searching for new sources of *CP* violation has become an attractive focus in the quest for new physics.

The observation of *CP* violation implies time-reversal symmetry *T* violation (and vice versa) through the *CPT* theorem. This theorem asserts that field theories with local, Lorentz invariant and hermitian Lagrangians must be invariant under the combined transformation *C*, *P*, and *T*. In the absence of degeneracy, the energy of a spin-½ particle, e.g., a neutron, in an electric field *E* is related to $d_n$ by $E_n = d_n \boldsymbol{\sigma} \cdot \mathbf{E}$ where $\sigma$ is its Pauli spin matrix. Because this expression is odd under *T* (and *P*), measuring a nonvanishing $d_n$ is also a unique signature for *CP* violation. The same arguments apply to the electron EDM, $d_e$,—whose value is determined from measurements of the EDM of paramagnetic systems, i.e., those having unpaired electrons, such as atomic thallium—and to the EDM of diamagnetic atoms such as $^{199}$Hg or $^{129}$Xe.

Importantly, the EDMs of each of these systems carry a complementary dependence on the *CP* violating parameters of a given new physics model. For example, $d_e$ is quite insensitive to *CP* violation in the strong sector, making systems with quarks the only viable probe of strong *CP* violation. In contrast, the neutron, lepton, and neutral-atom EDMs generally depend differently on the complex phases entering any new EW *CP* violation. Consequently, it is essential to carry out measurements in a variety of systems in order to provide the most comprehensive probe. Moreover, if a nonzero EDM is observed, then it will require complementary EDM measurements to discern the source of the new *CP* violation among the many possibilities. In this respect, the time is ripe for a new $d_n$ search with significantly greater sensitivity, as complementary efforts are currently underway for $d_e$ and neutral-atom EDMs.

*CP Violation and the Baryon Asymmetry of the Universe*

One of the outstanding puzzles of physics is the fact that the universe contains any baryonic matter at all. Indeed, if the universe were matter-antimatter symmetric at its birth, then one might expect the matter and antimatter in the universe should balance out in the present universe. The departure from this expectation is characterized by the baryon asymmetry, $\Delta n_{Bar}/(n_{\rm Bar} + n_{\overline{Bar}})$, where $\Delta n_{Bar} = n_{Bar} - n_{\overline{\rm Bar}}$ is the difference in the abundances of baryons and antibaryons. It is conventional to quantify this asymmetry in terms of the number of baryons in the universe today, $n_{Bar}|_{today}$, and the number of photons in the cosmic background $n_\gamma$. One observes that the ratio $r_{Bar} \equiv n_{Bar}|_{today}/n_\gamma$ is just a few $10^{-10}$, *i.e.*, that the universe is strikingly dilute, containing just a single baryon for every $10^9$ or so photons.

Of course, $n_{Bar}$ changes over time. During an earlier epoch, when the temperature of the universe was above the threshold for production of nucleons and antinucleons ($T \sim 10^{13}$ K), both species were plentiful and were in thermal equilibrium with the photons. The photon number, $n_\gamma$, is roughly constant in time [viii]. At that time, $\Delta n_{Bar} \approx n_{Bar}|_{today}$ [lxxxix]. The baryon asymmetry of the universe (BAU) at this earlier epoch is therefore approximately equal to the value of $r_{Bar}$,

$$\frac{\Delta n_{Bar}}{n_{Bar} + n_{\overline{Bar}}} = r_{Bar} \approx \text{ few} \times 10^{-10}. \qquad \text{(I.1)}$$

The basic question is: how could this BAU result from physical processes happening since the birth of the universe in the Big Bang some $\tau_U \sim 10^{10}$ years ago?

In a seminal paper, A. Sakharov [ix] identified three ingredients that would have to have been present in the particle physics of the early universe in order to account for the BAU:

(1) reactions that change baryon number have to occur;
(2) these reactions must be both *C* and *CP* violating; and
(3) they must occur in nonequilibrium processes.

Attempts to understand the BAU from this point of view—known as baryogenesis—have focused on several eras of cosmic evolution:

(1) One—the era of grand unified theory (GUT) baryogenesis—occurred when the temperature of the universe was $T \approx 10^{29}$ K, corresponding to an energy scale $M_x \approx 10^{16}$ GeV. If the forces of nature were unified at the beginning of cosmic evolution, then it is believed that the unification of the

strong and EW interactions would have begun to break down at this time. In this scenario, the BAU is produced in tandem when the symmetry group for grand unification was spontaneously broken.

(2) At the other extreme, baryogenesis could have occurred during the era of EW symmetry breaking when it is thought that the particles of the SM became massive. This era corresponds to $T \approx 10^{15}$ K or energies of about 100 GeV comparable to the mass of a $W$ or $Z$ gauge boson. We discuss this possibility of EW baryogenesis (EWB) [x] in more detail below.

(3) A third possibility involves neutrinos in the early universe. If at some temperature, well above the EW phase transition, an excess of leptons over antileptons is generated, topological processes that conserve baryon minus lepton number, can communicate this asymmetry to the baryon sector [xi]. This scenario—known as leptogenesis—has seen considerable interest recently, generated by the observation of neutrino oscillations. The most natural explanation for the nonvanishing, but tiny, neutrino mass implied by these oscillations is the existence of a heavy, Majorana neutrino that mixes with Dirac neutrinos to generate small masses via the seesaw mechanism. Because Majorana neutrinos are their own antiparticles, their interactions violate total lepton number. Thus, out-of-equilibrium decays of the heavy Majorana neutrinos in the early universe could have created the lepton asymmetry needed for the BAU—provided there exists new *CP*-violation in the lepton sector.

While all three of these possibilities are theoretically attractive, only the second option—EWB—can be tested and (in principle) ruled out experimentally. Generally speaking, the mass scales associated with particles in GUT baryogenesis and leptogenesis are too large to make their effects discernible to experiment. Moreover, the *CP* violation associated with these heavy particles need not be manifest at low energy. For example, the analog of the phase factor $e^{i\delta_{CKM}}$ that arises in the mixing matrix for the light neutrinos could be identically zero, even if the *CP* violating phases needed for leptogenesis processes at high energies were large enough to explain the BAU. Observation of a *CP* violation in the light neutrino sector would provide indirect evidence for the viability of leptogenesis. In contrast, EWB involves new particles with masses of order the EW scale, and the connection between the *CP* violating interactions of these particles and the *CP* violation needed to explain the BAU is more direct than in the high scale baryogenesis alternatives. Thus, EDM searches—at the level of sensitivity expected for this nEDM experiment—are poised to discover this new electroweak *CP* violation if EWB is responsible for the BAU.

Theoretically, EWB has seen a resurgence of scrutiny recently after the first generation of studies in the 1980s and 90s. During that time, Shaposhnikov [xii] analyzed EWB in the SM and showed that—while the SM contains all of Sakharov's ingredients—they are not sufficiently effective to account for the BAU. In the SM and other non-Abelian gauge theories there exist multiple and topologically distinct vacuum states distinguished by their baryon number and lepton number. Although baryon current conservation strictly forbids transitions among states of different baryon number states at the classical level, one finds quantum mechanically that the divergence of the baryon current is subject to triangle anomalies that signify symmetries broken at a quantum mechanical level. Thus, baryon-number-violating transitions are no longer forbidden, and the corresponding probability may be expressed in terms of instanton-like gauge field configurations [xiii] called sphalerons. This probability is extremely small for $T \approx 0$ as in the universe today where the proton lifetime $\tau_p > 10^{32}$ yr >> $\tau_U$; however, when the temperature is greater than ~$10^{17}$ K, sphalerons are easily excited, and anomalous baryon number violation is extremely rapid [xiv]. In this way, the first Sakharov condition is satisfied in the SM. The second Sakharov condition is satisfied in the SM through the explicit *CP*-violation present in the CKM matrix. Finally, if conditions of supercooling prevail at EW-scale temperatures, then the third Sakharov condition is satisfied in the first-order transition, occurring as droplets of the broken phase begin to nucleate out. Supercooling refers to the situation where the universe cools through expansion beyond the point at which a phase change would already have occurred under equilibrium conditions.

However, Shaposhnikov [xii] was unable to describe $r_{Bar}$ quantitatively in the SM. The SM has two shortcomings. First, the SM *CP*-violating effects are highly suppressed by the small mixing angles of the CKM matrix and light fermion Yukawa couplings. As a result, the largest BAU that might be created

via SM processes is many orders of magnitude too small. Second, it is now believed that a single Higgs doublet as incorporated into the SM would not support a first-order electroweak phase transition because a single Higgs doublet with mass, $M_H > 70$ GeV is known, from lattice gauge calculations [xv], to be insufficient for supercooling, and at the same time LEP measurements imply that $M_H$ exceeds 114.4 GeV. Clearly, new physics beyond the SM, including new sources of *CP* violation that may lead to a measurable value for $d_n$, must exist if the observed BAU arises from EW baryogenesis.

One such source might be found in the supersymmetric extensions of the SM. It has been shown recently [xvi,xvii,xviii,xix,xx,xxi,xxii,xxiii,xxiv] that small values of the *CP* violating phases (consistent with constraints from $d_n$) can provide values of $r_{Bar}$ comparable to the empirical value given in Equation I.1. In many SUSY models, both the BAU and the EDMs of elementary fermions depend on two CP violating phases: $\phi_\mu$ and $\phi_A$. The baryon asymmetry is then given by

$$r_{Bar} = F_1 \sin\phi_m + F_2 \sin\left(\phi_m + \phi_A\right) \tag{I.2}$$

where $F_{1,2}$ are functions of the other supersymmetric parameters. For suitable choices of these parameters, the production of baryon number can be enhanced through resonant scattering of superpartners from the spacetime-varying Higgs vacuum-expectation values during the phase transition. Near the peaks of these resonances, a sufficiently large BAU can be produced for values of the *CP* violating phase $\phi_\mu \sim$ few times $10^{-2}$; precision EW data prevent the $F_2$ term from becoming resonantly enhanced.

The presence of $O(10^{-2})$ phases is marginally compatible with present EDM limits and one-loop contributions from superpartners. An illustration is shown in Figure I-2, where the constraints on the phases $\phi_\mu$ and $\phi_A$ from present $d_e$ and $d_n$ limits are shown for representative choices of SUSY mass parameters [xxi]. The colored band indicates the region needed to produce the BAU. Figure I-2 illustrates both the complementarity of the neutron and electron EDM measurements for this particular scenario as a probe of new *CP* violation. Moreover, the impact of improved precision is clear. As the sensitivity of the measurements is increased by two orders of magnitude, the width of the EDM bands will shrink by similar factors, as the EDMs depend linearly on the *CP* violating phases. If resonant superesymmetric EWB is responsible for the production of the BAU, then future measurements should discover a nonvanishing EDM. Conversely, the absence of a signal would rule out this particular scenario.

It is important to bear in mind that Figure I-2 applies to one particular SUSY scenario, and that the dependence of both EDMs and the BAU on *CP*-violating phases in other scenarios can be considerably more complex. In versions of SUSY with an extended Higgs sector, for example, resonant enhancements of $F_2$ may be allowed, leading to a stronger dependence on the phase $\phi_A$. In this case, exploiting the complementary dependence of $d_e$ and $d_n$ on the *CP*-violating phases would be crucial to probing such a scenario. Considerable theoretical work remains to be undertaken to study *CP*-violation and baryogenesis in this broader class of models, and the new EDM measurements provide theorists with strong motivation to carry out this analysis.

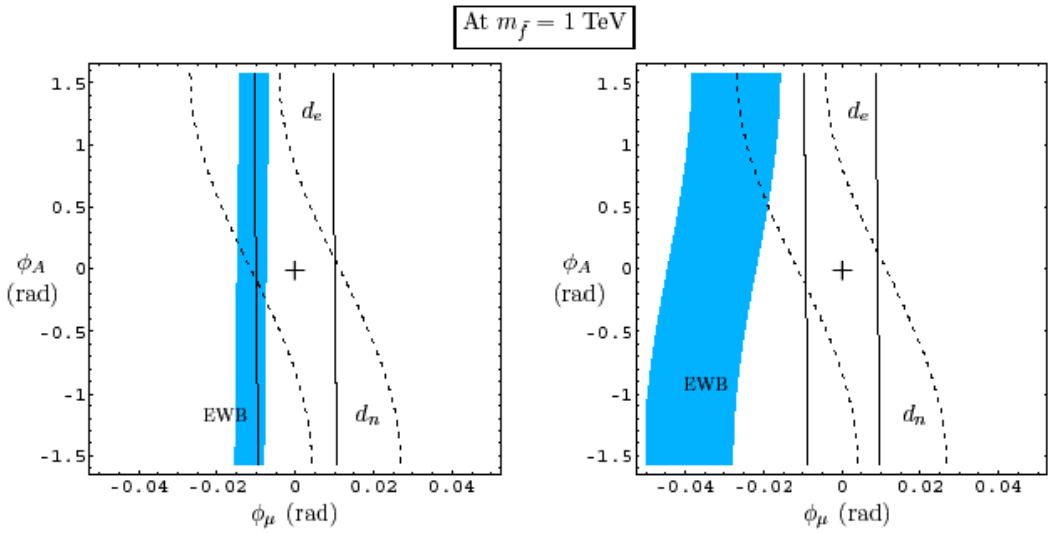


Fig. I-2.The role of $d_n$ and $d_e$ in determining the phases of EWB for representative parameter choices in the supersymmetric theory. The blue band is the choice of parameters to explain EWB. The dotted band is the limit for $d_n$ and the solid band is the limit from $d_e$. The plots represent two different choices of SUSY mass parameters.

The one-loop EDM constraints on SUSY *CP* violation can be evaded if some of the supersymmetric particles are sufficiently heavy. Recently, there has been considerable interest in a variant on SUSY known as "split supersymmetry"—wherein the masses of the fermion superpartners are quite large (of order 10 TeV or more) while the masses of the gauge and Higgs boson superpartners that make up charginos and neutralinos remain of order the EW scale. In this scenario, the EDMs of the neutron and electron arise at two-loop order, and the constraints on the *CP* violating phases are more relaxed. In particular, phases of O(1) are not presently ruled out for split SUSY, and there exists considerable latitude for resonant EW baryogenesis to produce the BAU.

The impact of present and future EDM measurements on the viability of this scenario is illustrated in Figure I-3 (see Reference [xxiv]), where the constraints are shown on SUSY mass parameters obtained by effective baryogenesis, LEP 2 direct-search bounds, and two-loop electron EDM limits (the implications of $d_n$ are similar). The parameters $\mu$ and $M_1$ govern the masses of the Higgs and guage boson superpartners, respectively. The light-blue bands give the region required by resonant EWB for $\sin\phi_\mu = 0.1$. The red region is excluded by LEP2. The region below the dark-blue line is ruled out by present bounds on $d_e$. The remaining bands indicate the prospective reaches for future experimental $d_e$ probes (similar to those for the neutron). Again, as in the case of the conventional SUSY scenario, future EDM measurements have the potential to exclude resonant SUSY baryogenesis if an EDM of order $10^{-28}$ $e$·cm or larger is not discovered. It should be noted that the precise bands associated with nEDM measurements are not shown, as there exist differences in the literature over the relative signs of various two-loop contributions. Theorists are addressing these disagreements—motivated in part by the new $d_n$ measurement discussed here. Nevertheless, the overall order of magnitude sensitivities of the electron and neutron EDM measurements to two-loop effects are comparable.

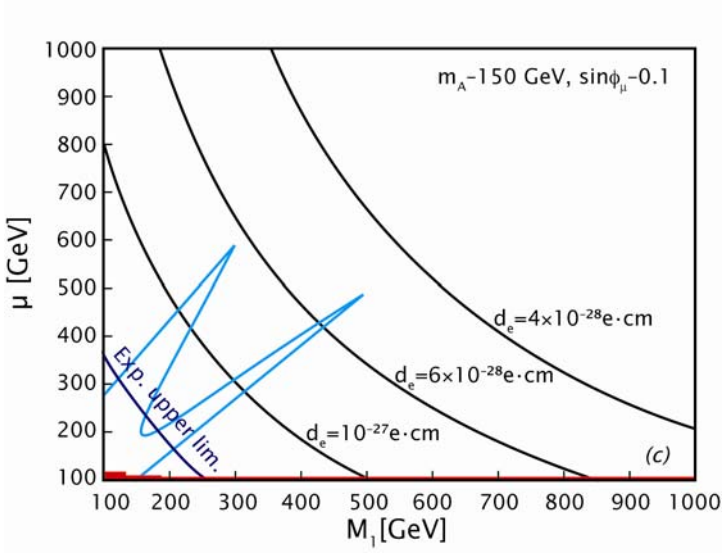


Fig I-3. The allowed space for the Higgs and *W* boson superpartners for a particular SUSY model. The allowed band is to the upper right of the limits on $d_e$ (solid lines) and LEP 2 direct searches (dark blue). The values required for EWB with $\sin\phi_\mu$ =0.1 are toward the origin (light blue).

In short, the nEDM experiment proposed here, together with other concurrent EDM measurements on complementary systems, will be a powerful probe of cosmology. One might ask how robust this probe will be during the era of studies at the Large Hadron Collider (LHC). To address this question, Figure I-4 shows the reach of various collider studies into the parameters space shown in Figure I-3. The light blue and red bands are as in Figure I-3. The grey region is excluded by the requirement that the lightest supersymmetric particle (LSP) be a neutralino and, thus, a candidate for cold dark matter. The prospective reach of the LHC is indicated by the green lines and arrows, while the possible reach of a future linear collider is given by the blue curves. As one can see, the LHC will probe some—but not all—of the parameter space relevant to baryogenesis in this scenario, even if one requires the neutralino to be the LSP. Indeed, the lower portion of the light blue bands could still be allowed and imply observable EDMs after completion of LHC running.

*Strong CP*

As noted above, the SM contains two sources of *CP* violation. In the EW sector it appears through $\delta_{CKM}$. The other is a term in the QCD Lagrangian itself, the so-called $\theta$-term,

$$L_{\mathrm{QCD}} = L_{CP} + \frac{\bar{\theta} g_s^2}{32\pi^2} G_{\mu\nu}\tilde{G}^{\mu\nu}, \qquad \text{(I.3)}$$

which explicitly violates *CP* symmetry because of the appearance of the product of the gluonic field operator *G* and its dual $\tilde{G}$. Because *G* couples to quarks but does not induce flavor change, $d_n$ is much more sensitive to $\theta$ than it is to $\delta_{CKM}$; additionally, the $\theta$-term is practically irrelevant to $d_e$ and kaon decays. Thus, measurement of $d_n$ would uniquely determine an important parameter of the SM. Calculations [xxv,xxvi] have shown that $d_n \sim \mathrm{O}(10^{-16}\theta)$ $e$·cm.

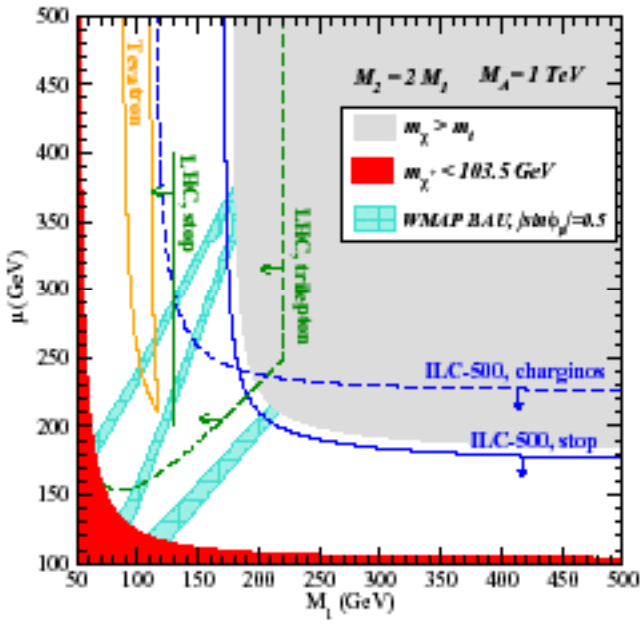


Fig. I-4.Physics reach of present and future collider studies relevant to SUSY baryogenesis. The light-blue and red regions are as in Figure I-3. Yellow lines indicate prospective sensitivity of Tevatron studies. Green lines indicate parameter space accessible to LHC measurements. The reach of a 500 GeV ILC is shown by the blue lines.

Although the value of the strength $\theta$ is unknown, the observed limit on $d_n$ implies that $\theta < 10^{-9\pm1}$ [xxvii]. A comparable limit on $\theta$ comes from the EDM of the mercury atom. However, the natural scale apparent in Equation I.3 suggests rather that $\theta \sim$ O(1). The extreme smallness of $\theta$ (The so-called strong *CP* problem) begs for an explanation. One attempt [Reference xxviii] augments the SM by a global U(1) symmetry (referred to as the Peccei-Quinn symmetry) imagined to be spontaneously broken and to give rise to Goldstone bosons called axions. The $\theta$-term is then essentially eliminated by the vacuum expectation value of the axion. Subsequently, much experimental effort and millions of dollars have been spent on the search for axions. The fact that axions have not been observed is, however, not in conflict with the empirical limit on the $\theta$ because the allowed axion parameter space has not yet been completed explored experimentally. Moreover, other proposals exist [xxix] to explain the small value of $\theta$. For example, if *CP* violation is implemented spontaneously, $\theta = 0$ as the leading effect arises naturally. Clearly, an experimental determination of $d_n$ has the potential to lead to a new paradigm for *CP* violation.

*Electroweak CP*

In any case, because *CP* violation as represented in the CKM matrix embodies flavor mixing, $d_n$ is very small in the SM; calculations predict it to be $10^{-32}$ to $10^{-30}$ $e$·cm [xxx,xxxi], well beyond the reach of any experiment being considered at present. Because of the experimental evidence indicating the presence of direct *CP* violation, a pure $\Delta S = 2$ interaction is insufficient to impact experiments. As $d_e$ cannot originate in the SM even from three-loop diagrams, the prediction of the SM, $d_e$ (SM) $< 10^{-40}$ $e$·cm [xxxii], is also well beyond current experimental capabilities.

Models of new physics, including left-right symmetric models, nonminimal models in the Higgs sector, and supersymmetric models as discussed above, allow for *CP*-violating mechanisms not found in the SM, including terms that do not change flavor. For this reason, searches for $d_n$ and $d_e$—for which the effects of flavor changing *CP* violation are suppressed as in the CKM case—have been significant for the development of such models. The models allow for effects that might be observed in a variety of

experiments including the new searches for $d_n$ and $d_e$, *B*-meson decay, transverse polarization of muons in $K_{\mu 3}$ decay; decays of hyperons; decays of $\tau$ leptons; and *CP* violation in charmed hadron decays.

If the origin of *CP* violation is essentially correctly described in the SM through $\delta_{CKM}$, large characteristic *CP* asymmetries are predicted for *B*-decay [xxvii]. Recent results from the *Belle* and *BaBar* collaborations present compelling evidence for *CP* violation in the neutral *B* meson system roughly consistent with these expectations [xxxiii]. However, the large, *CP*-violating effects in *B*-decay arising in the SM could be obscuring signals of new physics that would be manifest otherwise in these decays. In this case, the fact that *CP* violation arising from the CKM matrix is very small in $d_n$ leaves open the possibility that measurable effects will be found in $d_n$ even if further analysis finds no deviation from the SM in *B* decays.

More generally, models of new physics contain sources of *CP* violation that affect both flavor-changing and flavor-conserving sectors with a relative weighting characteristic of the model. Correlations between flavor-changing and flavor-nonchanging observables (such as between *B*-decay and EDMs) can provide important clues to distinguish among competing theories.

*Models of New Physics*

As the discussion of the baryon asymmetry indicates, there exists strong motivation from the standpoint of cosmology to search for new sources of *CP* violation. The level of sensitivity needed to probe *CP* violation at a cosmologically significant level is indicated by the EDM-baryogenesis bands in Figures I-2, I-3, and I-4. It is similarly useful to consider the implications of the nEDM experiment for other models of new *CP* violation. As illustrated above in the case of SUSY, such models provide a natural and reasonable expectation that the values of $d_n$ may lie at levels just beyond current empirical limits. Additionally, these models clearly show that significant correlations among different *CP* measurements can be expected, and that knowledge of these correlations is essential to unraveling the origin of the effects once they are found. If $d_n$ is *not* seen at levels just beyond current empirical limits, one would arrive at the important conclusion that something quite special is going on.

In the following discussion of models, we focus on $d_n$, but it is important to bear in mind that the EDM of atoms (see below) and of the electron are also relevant. In many models, $d_e$ is predicted to lie at least an order of magnitude below $d_n$. The reasons for this are the smaller chirality flip and weaker gauge couplings for leptons [xxxiv]. However, there is a great deal of model dependence, and in the absence of experimental information, $d_e$ or $d_n$ may be favored by the specific choice of parameters. In parallel to efforts to improve the experimental sensitivity to $d_n$, ambitious attempts to improve on the electron EDM measurements are being vigorously pursued. These efforts include a measurement on an excited metastable state of PbO [xxxv] in which a factor of $10^4$ improvement in statistical sensitivity is being sought and a measurement of the change in magnetization of solid-state systems such as GdIG or GaGd garnet upon application of electric field [xxxvi] in which a factor of $10^5$ improvement is possible. Based on experience with these theoretical models and the current empirical limits, one may infer that new experiments to measure $d_e$ or $d_n$ would have to exhibit about the same improvements in sensitivity over existing measurements to be competitive. In the case of neutral atoms, various nuclear-structure effects are expected to amplify the impact of *CP* violation (see Reference [xxxvii] and references therein), so new experiments with sensitivity comparable to that of the $^{199}$Hg measurement will effectively probe this *CP* violation with a sensitivity comparable to that of the new $d_e$ and $d_n$ measurements.

Among models, one leading candidate, SUSY, has already been discussed above. In addition, left-right symmetric gauge models [xxxviii] have many intriguing features such as the highly symmetric starting point that motivates them. Although many potential dynamical sources of *CP* violation exist, the EDM in these models is driven by $W_L$–$W_R$ mixing, the scale of which is set by the mass of the $W_R$ boson. These models are interesting because they show that it is possible, through $W_L$–$W_R$ mixing, to have $\varepsilon'$ agree with neutral kaon decay, yet have $d_n$ large enough to be observable (at the level of $O(10^{-27})$ $e$·cm [xxvii]). The electron EDM can be naturally in the range of $10^{-26}$ to $10^{-28}$ $e$·cm [xxxiv]. The most strict limits on the relevant parameters in these models [xxxix] have been determined from measurement of the EDM of diamagnetic atoms (atoms with paired electrons such as $^{129}$Xe and $^{199}$Hg). Diamagnetic

systems are sensitive to *CP* violating effects predominantly through the nuclear force rather than through $d_e$ [see, e.g., Equation (I.4), below].

*CP* violation in the CKM matrix of the SM may also occur "minimally" via the complex couplings of the Higgs to the fermions. A class of nonminimal models arises in the Higgs sector through *CP* violation generated from spontaneous symmetry breaking. There is considerable latitude in constructing these models, because the Higgs sector represents the largest area of unknown physics of the SM and lacks direct experimental support. As with other models, such as SUSY, the origin of an EDM in multi-Higgs models can lie in one of several sources:

(1) Higgs exchanges that generate an EDM for individual quarks $d_q$ or leptons. Such direct one-loop contributions with charged Higgs, tend to give a large $d_n$ incompatible with experimental upper limits, if one insists that the empirical value of $\varepsilon$ also originates entirely within this sector [xl]. Thus, for these models to be viable, one must arrange for $\varepsilon$ to arise in part (or entirely) from other sources (such as the CKM phase).

(2) *CP* odd gluonic operators that induce a $d_n$. Because the contribution of these operators is suppressed by successively higher powers of $M_H$ with increasing operator dimension, the operator most likely to give the dominant contribution to $d_n$ (excluding $G\tilde{G}$, which is related to $\theta$ as discussed earlier) is $G^2\tilde{G}$. Estimates for the resulting $d_n$ suggest values $d_n \sim \mathrm{O}(10^{-26})\ e\cdot\mathrm{cm}$ [xli,xlii].

(3) Quark color-electric dipole moments, $d_q^{QCD}$, (two-loop effects) that lead to large $d_n$ with values close to the current upper bound [xli,xliii,xliv]. The corresponding two-loop contribution to $d_e$ is obtained by replacing gluons in the color-electric dipole operator by EW gauge bosons and attaching them to a lepton. This yields $d_e \sim$ few $10^{-27}$ [xli,xliii,xliv,xlv,xlvi] which is just at the present experimental bound.

Recognizing that this classification is actually quite general and applicable in particular to supersymmetric theories [xlvii], the EDM of the neutron and the paramagnetic atom *Tl* can be expressed in terms of quantities appearing in this classification as [xlviii,[xlix]]

$$d_n = 1.1\left(\frac{4}{3}d_d - \frac{1}{3}d_u\right) + O(1)d_q^{QCD} + O(1)(q/10^{-9})d_n^{2005}$$

$$d_{Tl} = -600d_e + O(10^{-4})d_q + O(10^{-3})d_q^{QCD} + O(10^{-3})(\theta/10^{-9})d_{Tl}^{1995} \qquad \text{(I.4)}$$

where the expressions for the neutron have been taken from the QCD sum rule analysis of reference [xlix].

Corresponding relationships exist for the diamagnetic atoms; a typical result is

$$d_{Xe} = 10^{-3}d_e + O(10^{-4})d_q + O(10^{-3})d_q^{QCD} + O(10^{-1})(q/10^{-9})d_{Xe}^{1995}. \qquad \text{(I.5)}$$

In these expressions, the contribution from strong *CP* violation involving the $\theta$-term, has been expressed in terms of the current upper bounds ($d_{Tl}^{1995} \le 6.610^{-24}\ e\cdot\mathrm{cm}$, $d_{Xe}^{1995} \le 1.410^{-26}\ e\cdot\mathrm{cm}$, and $d_n^{1995} \le 0.810^{-25}\ e\cdot\mathrm{cm}$). A recent analysis [l] within the context of the MSSM has shown that the measurement [li] of the EDM of $^{199}$Hg may be providing the most reliable constraint on *CP*-violating phases.

Thus, one cannot rule out the possibility that nonminimal Higgs models will lead to values for $d_n$ and $d_e$ that are observable with the improvements in sensitivity planned in next-generation experiments. These models may also make significant contributions to other *CP* violating observables, such as the transverse polarization in $K_{\mu 3}$ decay, without necessarily having much effect on kaon decays. They are especially worthy of attention because Higgs dynamics also appears to be capable of providing sufficient *CP* violation to generate the BAU of today's universe at the EW scale.

Within each scenario, there can be numerous nontrivial correlations among the *CP* observables, rare decay rates, and gross features of the particle spectrum; for example, in the SO(10) GUT, $d_n$ and $d_e$ scale as $1/m^2$ with the scale $m$ of supersymmetry breaking, whereas the $\mu \rightarrow e\gamma$ rate scales as$1/m^4$ [lii].

*Summary and Conclusions*

There is ample reason to expect a nonzero value for the nEDM, with many theories predicting values lying within the six orders-of-magnitude window between the current limit and the value allowed by the SM. Experiments that explore the next two orders of magnitude would make a significant contribution to the search for new physics that complements the information to be gained from the Large Hadron Collider (LHC).

### A.1.c. EDM Experiments Worldwide

The history of nEDM measurements is closely interwoven with our evolving knowledge of discrete symmetries in physics. In 1950, when parity was considered an inviolable symmetry, Purcell and Ramsey [ii] pointed out the need to test this symmetry via detection of a nEDM. They then carried out a pioneering experiment [liii,iii] setting an upper limit at $5 \times 10^{-20}$ $e$·cm for nEDM. The role of the baryon (proton, neutron, hyperons) EDMs in testing parity symmetry was extensively discussed in the seminal paper of Lee and Yang [liv], who cited the yet-unpublished nEDM result from Smith, Purcell, and Ramsey [liii,lv].

The discovery of parity violation in 1957 [lvi,lvii,lviii] prompted Smith et al. to publish their nEDM result [iii]. By this time, however, it was recognized [lix,lx] that *T* invariance would also prevent the neutron from possessing a nonzero EDM. Because no evidence of *T* violation was found even in systems that exhibited maximal parity violation, a nonzero nEDM was regarded as highly unlikely. However, Ramsey [lxi] emphasized the need to check *T* invariance experimentally. He also pointed out that Dirac's magnetic monopole violates both parity *(P)* and *T* symmetry. The experimental activities on the nEDM lay dormant until *CP* violation, directly linked to *T* violation via the *CPT* theorem [lxii,lxiii,lxiv], was discovered in 1964 [lxv].

The interest in the nEDM was greatly revived when a large number of theoretical models, designed to account for the *CP*-violation phenomenon in neutral kaon decays, predicted a nEDM large enough to be detected. Many ingenious technical innovations have since been implemented, and the experimental limit of nEDM was pushed down to $3 \times 10^{-26}$ $e$·cm, a six-order-of-magnitude improvement over the first EDM experiment [4]. Unlike *P* violation, the underlying physics for *CP* and *T* violation remains a great enigma nearly 40 years after its discovery. As discussed above, improved nEDM measurements will continue to provide the most stringent tests for various theoretical models and to reveal the true origins of *CP* violation.

*Concurrent nEDM Experiments*

The search for a nonzero nEDM continues at the ILL with a two-phased approach. Phase 1 develops their technique and hopes to obtain a sensitivity of $10^{-27}$ $e$·cm. Phase 1 is in advance of this project by several years. If no limitation is discovered, they will ask the ILL to construct a more intense cold-neutron beamline that should provide a statistical sensitivity of $10^{-28}$ $e$·cm, and this phase is on a schedule comparable to this project.

The arrangement is shown in Figure I-4 [lxvi]. The design features a superthermal source based on liquid helium (LHe) to produce UCNs well away from their neutron detectors, thus essentially eliminating cold-neutron-induced background counts. A description of the super-thermal mechanism is given in Section IV. The measurement employs the Ramsey method of separated oscillatory fields [lxvii]. To avoid the geometric phase effect (see Section VII), the measurement cells are protected with a superconducting shield to isolate the cells from external magnetic fields. The main precession field is generated with a solenoid that possesses good field uniformity. A key feature is the cell arrangement, which contains three cells (not shown). There are two outer high-voltage (HV) electrodes that are held at ground and two inner electrodes held at the same HV. The measurement cells are between the ground and HV electrodes. The

magnetometry cell is between the two HV electrodes and has no electric field, and hence cannot have an EDM effect. The precession of the neutrons from each of the three cells is measured independently. Magnetic fluctuations in the outer two cells are corrected for by the fluctuations in the inner cell. The design does not employ a comagnetometer, so the ability to correct for the spatial variations in the magnetic field is limited to the scale of the cells.

A new UCN source, based on the superthermal production process in solid deuterium, is under construction at the Paul Scherer Institute (PSI) [lxviii]. The current plan for measuring the nEDM involves moving the EDM apparatus from the previous ILL nEDM experiment to the PSI. Their plans to modify the apparatus to overcome the geometric phase effect that limited the device at the ILL are unknown.

The design of the experiment planned for an experiment at the Petersberg Nuclear Physics Institute (PNPI) is under construction. This experiment also uses a deuterium superthermal source. It also uses the Ramsey method and features eight cells with different electric fields. The cells are quite large to gain statistics and have many external magnetometers. This type of magnetometry has proven very challenging in the past.

There are rumors of a new nEDM experiment that measures the spin precession of the neutrons as they pass through a single crystal. The advantage of this approach is the enormous electric field produced by the lattice. Not many details are available, but crystal experiments in the past have had difficulty getting enough neutrons that pass precisely along the crystal axis and in controlling the $v \times E$ systematic because it is a beam experiment [lxix].

There are similar rumors of one or two Japanese nEDM efforts at either KEK or JPARC. No details are available.

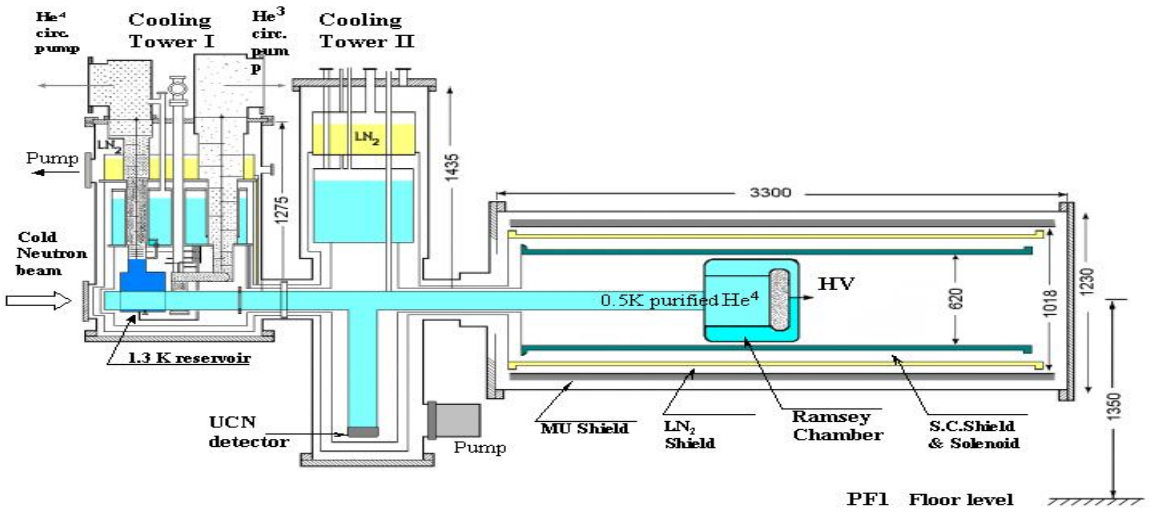


Fig. I-4.The experimental arrangement for the next neutron EDM experiment at the ILL.

*EDM Experiments in Diamagnetic Atoms*

Diamagnetic atoms have no unpaired electrons, and the major contribution to the EDM of the system comes from the nucleus. The atomic electrons screen the effects of the EDM. The nuclear EDM is only measurable because relativistic effects keep the cancellation between the nucleus and the electrons from being exact. As noted earlier, the nuclear contribution to the EDM is sensitive to different parts of the *T*-violating force as compared to the neutron. For example, $^{199}$Hg is about 100 times less sensitive to quark chromo-electric EDMs compared to the neutron, but is about 1,000-10,000 times less sensitive to elementary quark EDMs. In addtion, there are theoretical hurdles in converting diamagnetic EDMs into quark EDM or $\theta_{QCD}$ values. With these caveats, under some simplifying, model-dependent theoretical

assumptions, the atomic EDM is sometimes quoted in terms of a nEDM, however the measurement of the neutron and diamagnetic-atom EDMs actually provide independent information. The conversion factor depends on the atomic number of the nucleus.

A series of experiments has been carried out on $^{199}$Hg at the University of Washington. Their latest result gives $d_{Hg} < 2.1 \times 10^{-28}$ $e$·cm. For mercury, the conversion factor to $d_n$ is about 100, which translates into a limit on $d_n < 2 \times 10^{-26}$ $e$·cm [lxx]. This result is very close to the direct limit from the ILL experiment. Efforts continue to improve the mercury result, and another factor of 2 or so may be expected in the next few years. Orders-of-magnitude improvement seems unlikely in the near future.

The other important diamagnetic atom is $^{129}$Xe. The current limit is $d_{Xe} < 2 \times 10^{-26}$ $e$·cm. After applying the appropriate conversion factor, the value for $d_n < 2 \times 10^{-23}$ $e$·cm [lxxi]. A new experiment at Princeton with an expected sensitivity of $d_{Xe} \sim 10^{-30} - 10^{-31}$ $e$·cm is underway [lxxii].

A program is underway Argonne National Laboratory towards a measurement of the electric dipole moment of $^{225}$Ra [lxxiii]. This experiment will take advantage of the expected enhancement of the atomic EDM of $^{225}$Ra due to the octupole deformation of the $^{225}$Ra nucleus. Currently, the feasibility of laser trapping and cooling of $^{225}$Ra atoms is being investigated.

*Electron EDM Experiments*

In theories of the weak interaction, the EDM of the electron is zero in first order, and, as discussed above, the electron EDM is sensitive to different parts of the *T*-violating interaction. There have been a number of precision measurements of the EDM of paramagnetic atomic and molecular systems, from which limits for the EDM of the electron can be inferred. For example, the measurements in thallium by Commins et al. [lxxiv] suggest a value of $d_e = (0.18 \pm 0.12 \pm 0.10) \times 10^{-26}$ $e$·cm. This experimental limit is about 13 orders of magnitude above the SM predictions, but some extensions for physics beyond the SM predict effects within range of these experiments.

Polar molecules offer the opportunity for large atomic enhancement factors. There are two examples currently being investigated. The first is YbF, where an upper limit of $d_e < 4 \times 10^{-25}$ $e$·cm has been reported by the Sussex group [lxxv]. The group continues to work with a hoped for sensitivity of $10^{-28}$ $e$·cm. The other system is PbO. The work at Yale is supposed to be at an advanced stage. The Yale team hopes for a sensitivity of $10^{-30}$ $e$·cm [lxxvi].

The work in polar molecules depends on detailed molecular structure. A rather different approach has been taken by a Los Alamos group investigation of GaGd garnet [lxxvii]. The idea is to place high voltage on an amorphous sample of the garnet and look for a very weak induced magnetic field. Noise is suppressed by working at cryogenic temperatures, and the magnetic field sensor is a SQUID.

There are many examples of searches for $d_e$ in the proposal stage, but the details and their reach are still not public.

*Other Low-Mass Particles*

There are two experiments proposed on other low-mass particles, one to search for the EDM of the muon and the other to search for the EDM of the deuteron. Both use the *g-2* ring at Brookhaven National Laboratory. The muon is like a heavy electron, so the physics is related to $d_e$. The sensitivity being sought is $d_\mu < 10^{-24}$ $e$·cm [lxxviii]. While this value appears quite a bit less sensitive than the values for $d_e$, there are some special extensions to the SM where the EDM is enhanced due to the large mass of the muon. In the case of the deuteron, the sensitivity is supposed to be $d_d < 10^{-27}$ $e$·cm [lxxix]. The physics of $d_d$ is quite similar, though complementary, to that of $d_n$ (the up and down quark EDMs enter with different relative signs compared to the neutron), so there is little reason to expect this measurement to have the same discovery potential as the new initiatives on the neutron. Both of these proposals await approval from Brookhaven and the funding agencies.

## A.2 Proposed Measurement

### A.2.a Design Overview

We discuss below the techniques and apparatus for the nEDM experiment. Moving from an overview in this section, the various subsystems are summarized with particular emphasis on those work packages (WBS level 3) for which the NSF-funded collaborators are responsible. These work packages are listed in **Error! Reference source not found.** and indicated in the following sections with the notation, e.g., {Boston University}. Slightly older, but more details about individual components may be found at http://www.npl.uiuc.edu/exp/nEDM/NSFAppendices. The discussion concludes with a summary of sensitivity and systematic uncertainties.

This experiment is based on a technique to measure the neutron electric dipole that is qualitatively different from the strategies adopted in previous measurements. The overall method adopted here [lxxx] is to form a three-component fluid of neutrons and $^3$He atoms dissolved in a bath of superfluid $^4$He at ~0.5 K. Incident polarized neutrons from the 8.9 Å beamline of the FNPB facility at the SNS are effectively stopped by the superfluid $^4$He (transferring their energy and momentum to phonons) and trapped in a plastic measurement cell with a wall potential of ~ 150 neV. The neutron (and $^3$He) magnetic dipoles can be made to precess in the plane perpendicular to an external applied (magnetic) holding field, $B_0$. The determination of the nEDM results from a precision measurement of the difference in the precession frequencies when a strong electric field parallel or antiparallel to $B_0$ is applied. Application of this static electric field, $E_0$, changes the Larmor precession frequency of the neutron, $\nu_n$, in proportion to $d_n$. The precession frequency is

$$\nu_n = -\left[2\mu_n B_0 \pm 2 d_n E_0\right]/h \equiv \nu_0 \pm \Delta\nu/2 \qquad \text{(II.1)}$$

where the minus sign reflects the fact that $\mu_n < 0$. Thus, the frequency shift, $\Delta\nu$, generated by the reversal of $E_0$, is

$$\Delta\nu = -4 d_n E_0 / h\,, \qquad \text{(II.2)}$$

In the case of $B_0$ = 10 mG and $E_0$ = 0, the Larmor precession frequency is $\nu_0$ = 29.2 Hz. With $E_0$ = 50 kV/cm, the frequency shift is

$$\Delta\nu = -48\ nHz\ \frac{d_n}{1x10^{-27}\ e\cdot cm} = -1.6x10^{-9}\nu_0\ \frac{d_n}{1x10^{-27}\ e\cdot cm}\,. \qquad \text{(II.3)}$$

Note that it is the absolute frequency shift, $\Delta\nu$, that must be measured, not its fractional shift.

The neutron precession is not directly observable; we use the strongly spin-dependent neutron capture reaction

$$\vec{n} + {}^3\vec{He} \rightarrow p + t + 764\ keV$$

and observe the scintillation light generated by the proton and triton in the $^4$He bath. For example, for the ultra-cold neutrons in this measurement, with velocities of a few m/s, the cross section for spin-singlet capture is 5.5 Mb; that corresponding to triplet capture is about 200 times smaller. In the experiment we are effectively comparing the neutron and $^3$He precession rates. This comparison measurement assumes the neutral $^3$He atom has a negligible EDM, as expected for a diamagnetic atom of low atomic number [lxxx].

The overall figure of merit for nEDM experiments varies as $E_0\sqrt{N\tau}$, which can be derived from Equation II.2. The neutrons decay, implying that the measurement must be repeated many times. $N$ is the number of neutrons in the cell during a single measurement and $\tau$ is the duration of each measurement. The constant of proportionality depends on the experimental arrangement. The object of any design is to maximize these three quantities, which this experiment achieves as explained below.

The conceptual design for the proposed apparatus is shown in Figure 0.A. The picture is derived from a full 3-D engineering model that has been created to study whether all the scientific ideas can be realized in a single piece of equipment. The apparatus is divided into two parts, the lower cryostat where the measurement is made and the upper cryostat where the polarized $^3$He is injected and removed as well as where the refrigeration is done. The upper cryostat is where all services enter the system (except for the light guides - to be described later).

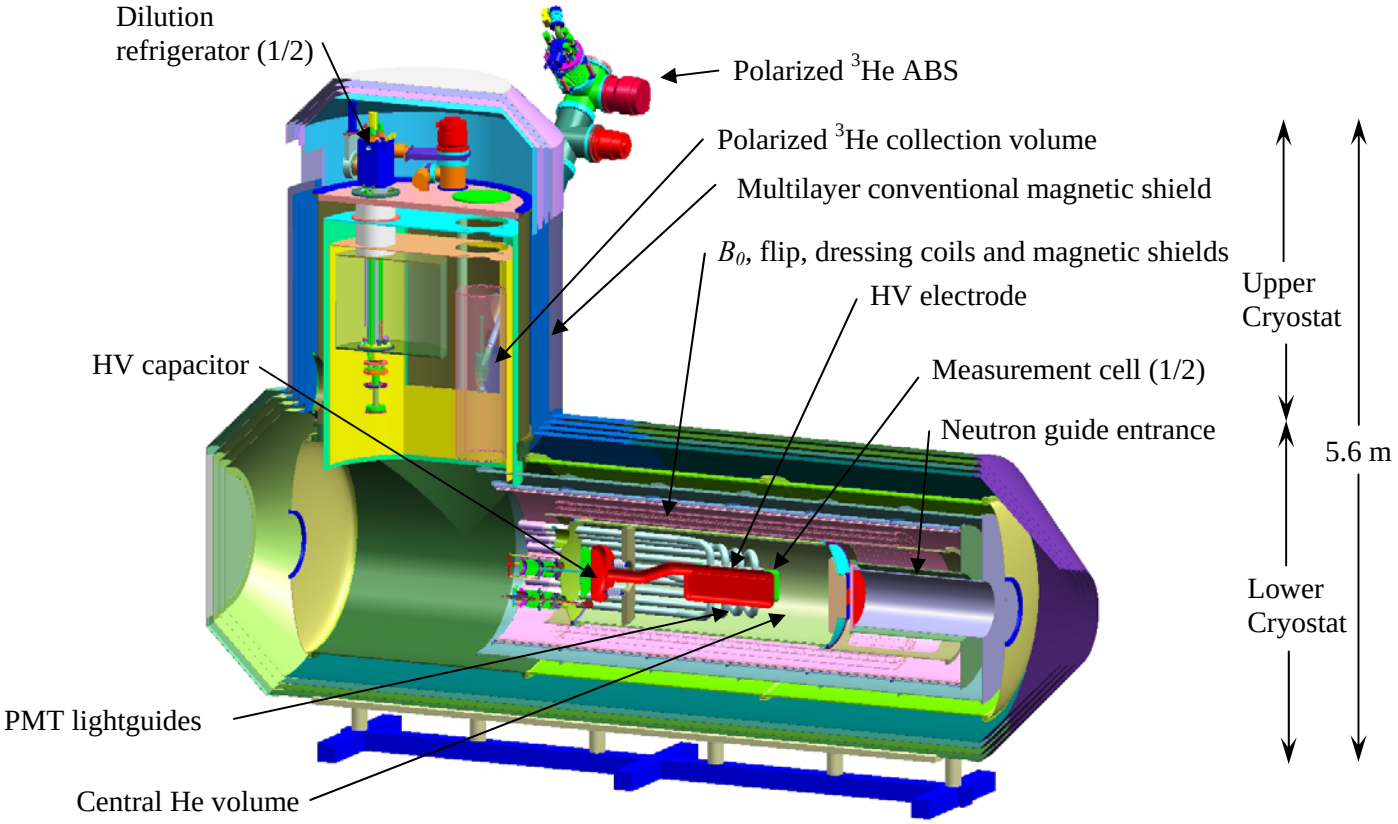


**Figure 0.A** The schematic overview of the full detector apparatus for the nEDM experiment. This view most clearly demonstrates the relationship between the upper and lower cryostats. The upper cryostat contains the refrigeration and $^3$He systems. The lower cryostat contains the entrance port for the neutrons, the magnets/magnetic shielding and the measurement cells.

### A.2.b Ultra-cold Neutron Production

The cold neutrons from the 8.9 Å beamline of the FNPB facility pass through a polarizing beam splitter which is the first element of the nEDM experiment (see Figure 0.C). The beam splitter utilizes multilayer magnetized supermirrors to provide, for a given spin state, a large transmission coefficient or a large reflection coefficient (see Figure 0.B). With this type of arrangement the neutrons are sorted from a single guide into two parallel guides by spin state and corresponding to the two measurement cells in the apparatus. The neutrons exit the polarizer with their spins vertical and in opposite directions in the pair of downstream guides.

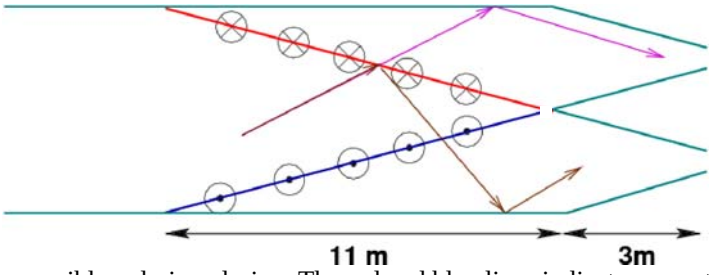


**Figure 0.B** Top view of a possible polarizer design. The red and blue lines indicate magnetically remnant polarizing sheets with antiparallel magnetization. The arrows are possible neutron trajectories for neutrons with spin iton the plane (violet) and out of the plane (gold).

The neutron spins in each measurement cell must be parallel to the horizontal holding field, otherwise there would be strong absorption of neutrons by polarized $^{3}$He atoms in one of the cells via the strong spin singlet capture process. Preparation of the correct spin orientation for the neutrons requires a spin-flip for the neutrons in one of the guides and then spin-rotation of the entire ensemble from vertical to horizontal {Indiana University}. For the purpose of determining systematic uncertainties, both downstream guides will be instrumented with spin-flip devices. The spin-flip may be done either with a resonant device in which the neutrons spend a particular amount of time in the r.f. field, or by using adiabatic fast passage, which is non-resonant, but requires a magnetic field gradient. In both cases, a substantial r.f. system is required to produce several hundred Watts with a frequency of tens of kHz, and, in addition, correspondingly high power switching. The two downstream guides (not shown in Figure 0.A) enter from the right and terminate roughly 50 cm upstream of the high voltage (HV) plates. The gap is necessary to preserve electrical stability. For the purpose of diagnostic measurements, particularly during the startup phases of the experiment, a neutron polarimeter and flux monitor will be built that can be inserted in the beamline just upstream of the cryostat {Indiana University}. Based on previous successful designs, the detector will utilize two ionization chambers and a magnetic supermirror enclosed by $^{6}$Li glass windows.

The lower cryostat contains two acrylic measurement cells sandwiched between a HV electrode and two ground electrodes as shown in Figure 0.D. These cells are loaded with ultracold neutrons (UCNs) using the strategy suggested first by Golub and Pendlebury [lxxxi] - superthermal production - a technique that produces a higher density of UCNs than any other. The UCNs are locally produced inside a cell filled

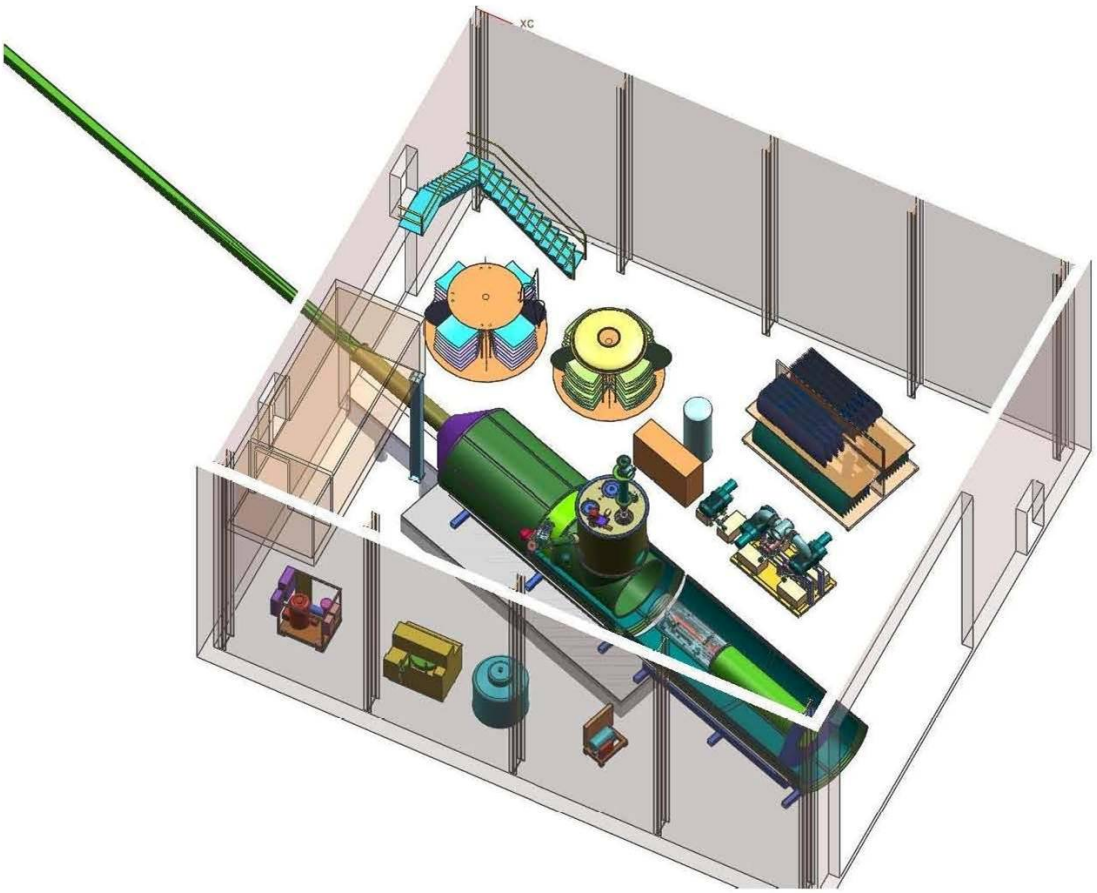

**Figure 0.C** The layout of the nEDM experiment at the FNPB. The cryostat is shown near the center of the UCN guide hall in an exploded view (segments of the conventional shield are stacked near the stairs). The downstream end of the 8.9 Å ballistic guide section is the dividing line between the FNPB and the nEDM experiment; beyond the ballistic guide, the neutrons pass through the beam splitter and polarizer on the way to the nEDM apparatus. The UCN building is also part of the FNPB.

with ultrapure, superfluid $^4$He at ~ 0.4 K. Cold neutrons with wavelengths of 8.9 Å (energies of 1 meV) can interact with the superfluid in significant numbers and be down-scattered to very small energies (less than the ~165 neV potential barrier of the measurement cell) with the recoil phonon carrying away neutron energy and momentum. At 0.4 K, the rate of up-scattering of UCN by phonons is negligible. The cold-neutron beam that traverses the cells is dumped in a boron nitride block downstream of the cells.

The averaged UCN production rate [lxxxii] at the SNS is about 0.3 UCN/cm$^3$/s and scales with the incident cold neutron flux. The measurement cells employ deuterated polystyrene coatings and a deuterated acrylic entrance 'window' to minimize neutron absorption by hydrogen [lxxxiii]. The goal for the mean life of a neutron in the measurement cell is 500 s considering losses from both neutron β decay and neutron/wall interactions. The neutron density will reach $\rho_n$ ~150 UCN/cm$^3$ during a 1000 s collection interval. This UCN production technique and the UCN production-rate calculations for a $^4$He filled UCN trap have been tested and validated by Golub, et al. [lxxxi] and by the neutron-lifetime experiment now in progress at NIST [lxxxiv].

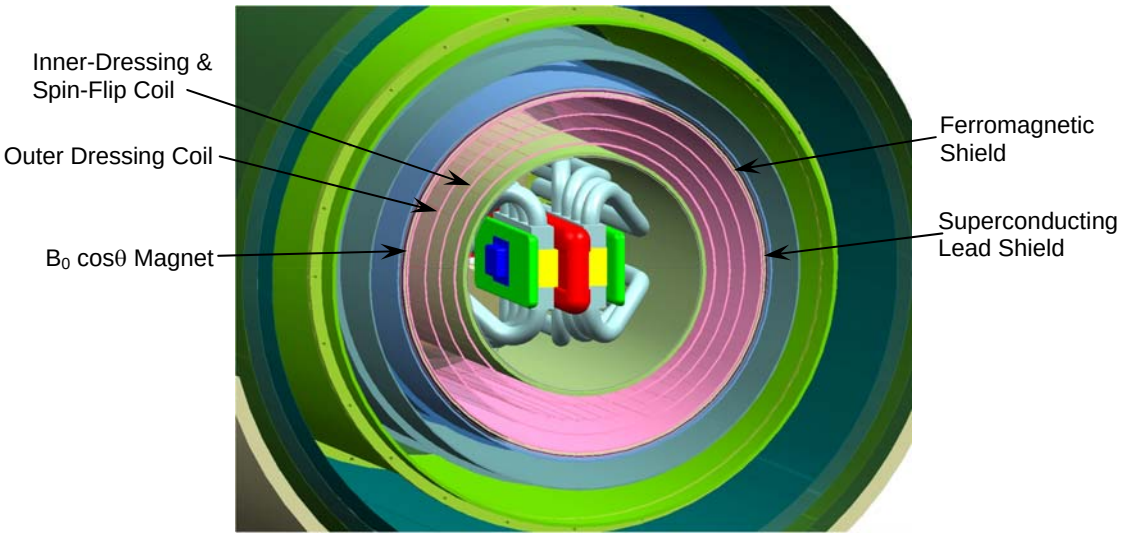


**Figure 0.D** The two measurement cells (yellow) surrounded by the HV electrodes (HV in red, ground in green), the lightguides (gray) and the SQUID packages (blue). In concentric circles from the inside to the outside are: HV ground return, inner dressing coil, all other magnet coils, ferromagnetic shield, superconducting shield, 4 K cryoshield, 50 K cryoshield and the outer vacuum jacket (tan). The conventional magnetic shield outside the vacuum jacket is not shown in this view.

### A.2.c Neutron precession measurement

The polarized $^3$He dissolved in the L$^4$He superfluid serves as an analyzer of the neutron precession rate. Scaled by the inverse of the neutron velocity from thermal values [lxxxv], the cross section for neutron absorption by $^3$He is about 5 Mb for spin the spin singlet state and about 200 times smaller for the triplet state (with higher order corrections at the 10% level). Thus, neutron absorption by $^3$He is highly spin dependent, and if the $^3$He concentration is adjusted to be about $10^{12}$ cm$^{-3}$, the neutrons are essentially absorbed only in the singlet state during the measurement cycle. The rate of neutron loss due to this absorption is

$$L_{n3} = \frac{N_{n0}}{\tau_3}\left(1 - P_n P_3 \cos\left[\left(\gamma_3 - \gamma_n\right) B_0 t + \varphi\right]\right) \qquad \text{(II.4)}$$

where $N_{n0}$ is the initial number of neutrons, $\tau_3$ is the spin-averaged absorption lifetime, the $P_i$ are the $^3$He and neutron polarizations and the $\gamma_i$ are the gyromagnetic ratios of the two species.

When a neutron is absorbed on a $^3$He atom, the reaction products are a proton and a triton that share 764 keV of energy. The reaction products produce scintillation light in the LHe that is emitted in the vacuum ultraviolet region. If the measurement cell is coated with a wavelength shifter, the scintillation light is converted to the blue where it may be viewed with photomultiplier tubes (PMT). The best wavelength shifter is deuterated tetraphenyl butadiene (dTPB) because it has good conversion efficiency and has a small neutron-absorption cross section [ref Lamoreaux paper]. The light guides that connect the cell to the PMTs exit the apparatus on the downstream end of the lower cryostat as shown in Figure 0.E.

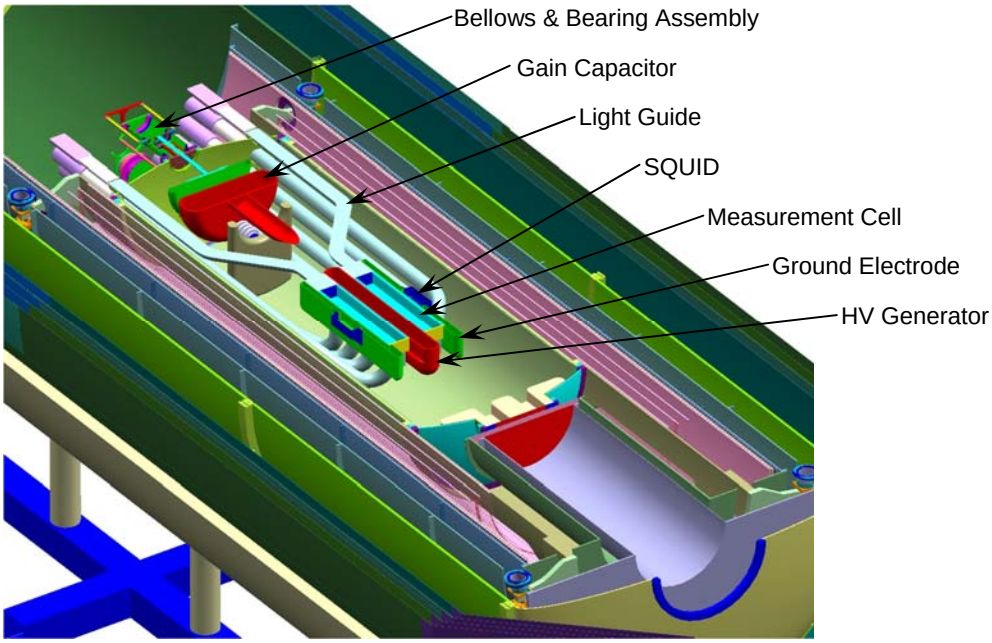


**Figure 0.E** A section of the central region of the nEDM apparatus showing the measurement cells, HV electrodes, the path of the lightguides and the HV capacitor system.

## A.2.d Magnetometry

Temporal or spatial variations in the magnetic field will be directly reflected in the neutron precession frequency. This problem can be overcome by introducing a second species that has no (or a much smaller) EDM and whose precession rate can be measured in the same volume so the variations can be removed [lxxx]. Data from the latest EDM experiment at the ILL illustrates the situation as shown in Figure 0.F [lxxxvi]. This experiment places polarized $^{199}$Hg near the neutron cell. The blue circles are the raw neutron resonant frequency. The non-statistical variations are clearly visible. The large step, near 15 hr, corresponds to an electric-field reversal. When the corrections are applied for the field variations measured by the $^{199}$Hg, the red circles are obtained; they are consistent with shot noise.

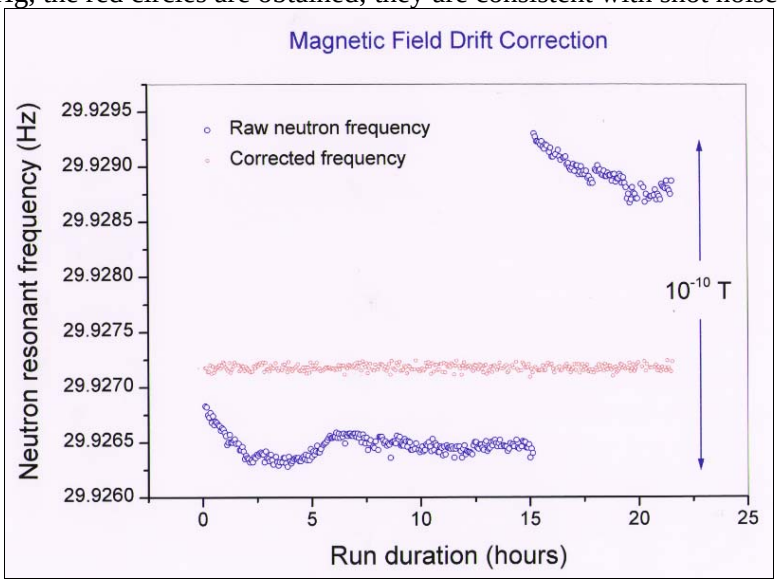


**Figure 0.F** Data from the recently completed ILL EDM experiment [1xxxviii]. The blue (red) circles are the EDM signal without (with) field corrections from the co-magnetometer.

The goal of the nEDM experiment is a factor of 100 improvement in the neutron EDM sensitivity. For an improvement beyond a factor of 3–10, magnetic field variations require improved. The optimal magnetometer to eliminate these field variations and many potential systematic errors is one that occupies the same volume as the neutrons. The collaboration has adopted this approach to overcome potentially insurmountable problems in achieving the goal. The only species that can coexist in the same volume as the LHe is $^3$He. It can have a polarization of nearly 100%; as a diamagnetic atom, it is expected to have an EDM less than that of $^{199}$Hg (whose EDM has an upper limit of $2\text{x}10^{-28}$ $e$·cm [Romalis]) because of the screening in light atoms [Schiff]. Except for the small gravitational-field-induced gradient in the neutron concentration, the $^3$He atoms will sample the same magnetic field as the neutrons. The precession rate of the $^3$He will measured with nearly conventional NMR, using SQUIDs rather than conventional pickup coils. Detection of the small $^3$He signal requires SQUIDS with a noise level ~ $0.2\ \mu\phi_0 / \sqrt{\text{Hz}}$ (commercially available). The SQUIDs are placed just outside the ground planes for the HV as shown in Figure 0.E.

## A.2.d Electric field

The electric field in the measurement cells is generated by what is essentially a parallel plate capacitor as shown in Figure 0.E. The electrodes are to be built from acrylic coated with a thin layer of carbon-based material, or from, e.g. pyrolytic graphite. A relatively small amount of charge is required to generate the appropriate field given the small (~50 pF) capacitance of the electrode system. There will therefore be a small charging current, and the carbon is an adequate conductor for this purpose. The electrodes will be bombarded by cold neutrons during the UCN production. Acrylic ($C_5O_2H_8$) and carbon are amongst a short list of materials that do not produce activated nuclei that decay by γ-ray emission with time constants comparable to the UCN storage time. It is crucial to minimize the decay γ rays that will Compton scatter in the measurement cell producing background scintillation light. The carbon conductor is also appropriate for minimizing the magnetic fields associated with thermal motion of electrons in materials with higher conductivity, such as metals, that would generate noise in the SQUIDs. The resistivity of the thin coating also minimizes the eddy-current heating generated by the radio frequency magnetic fields used in the experiment.

The electric field must be uniform and stable to 1% over the measurement cell to prevent systematic effects from entering. Distortion of the electric field due to the acrylic measurement cell is minimized by making an insets in the electrodes to recess the cell, effectively making the inside surfaces of the cell part of the electrode plane. The electric and magnetic fields must be aligned to within about $1^o$ which we believe should be straightforward with standard mechanical design. Leakage currents must be limited to about 1 nA to prevent electric-field-correlated magnetic fields. Such currents are roughly consistent with the bulk and surface resistivities of acrylic even at room temperature ($\rho \sim 10^{15}$ Ω·cm, $\rho_S > 10^{15}$ Ω·cm/cm; the breakdown strength exceeds 10 MV/m).

The apparatus must be designed to prevent all sparks because of the sensitivity of the SQUIDS. The HV electrode is contained in a cylindrical shell that also provides a ground reference. The ground shell must be situated at least 30 cm from the ends of the HV electrode to prevent sparks. The radius of curvature of the ends of the electrode also needs to be at least 5 cm to prevent sparking to the ground shell. This requirement sets the separation between the two cells to a minimum of 10 cm.

A potential difference of 350 kV is required to obtain a 50 kV/cm electric field across the 7 cm gap of the measurement cell {Indiana University}. Both LHe [1xxxv] and acrylic have the high dielectric strengths necessary to support this field. The capacitors within which each measurement cell sits, having capacitances of about 55 pF, and are charged by placing them in parallel with a variable capacitor with a

range of about 10 to 1000 pF. The variable capacitor is situated downstream of the neutron-beam absorber as shown in Figure 0.E. This variable capacitor, or HV multiplier, has a minimum plate separation of roughly 0.5 cm. It is charged with a power supply to 50 kV through a commercially available vacuum feed-through. The electrical conductor connecting to the power supply can have a small cross section and does not introduce a major heat leak into the cryogenics. Once the HV electrode is charged, the spherical contactor connecting it to the power supply is moved away from the electrode by means of a bellows. Once this separation occurs, the HV system is isolated from any power-supply ripple. The movable ground electrode with a similar bellows is then retracted to a distance of roughly 7 cm. Because the charge is conserved, the HV electrodes are raised to the desired 350 kV as the variable capacitance decreases (note that the decreasing total capacitance of the system is taken into account in determining the required motion of the variable capacitor).

The electric field will be regularly monitored between the variable capacitor plates using a generating voltmeter. Occasionally, the field will be determined in the measurement cells, by measuring the polarization rotation of visible laser light (Kerr effect) {Berkeley}. The rotation is proportional to the square of the electric field in the region; an accuracy of 1% in ~ 100 s is straightforward for these measurements [Budker]. Laser light will be transported to and from the cells using either polarization preserving optical fibers or with optical windows and mirrors.

Studies by the collaboration of the dielectric strength of superfluid He indicate that it may have a lower value than that of normal LHe, and that it may be compensated by an increase in pressure. The need to pressurize the LHe in the experiment to maintain the desired field would add significant complexity to the apparatus (as discussed briefly below), and this effect is being carefully studied in our R&D program before a final decision is made.

### A.2.e Scintillation detection

The reference design calls for light guides {Boston University} to carry the wavelength-shifted scintillation light out the downstream end of the apparatus to room temperature PMTs {Indiana University}. In this configuration, the PMTs should observe a mean of 12 photoelectrons for each capture, based on a very similar design employed at NIST [lxxxiv].

While this number of photoelectrons is sufficient to observe the scintillation light, it is not optimal for particle identification (ID), i.e., distinguishing the capture proton and triton from electrons generated either by neutron decay or Compton-scattered capture $\gamma$ rays. Because the sensitivity of the experiment depends on the ability to suppress backgrounds, alternate designs are still being evaluated. The particle ID depends on detecting the de-excitation modes of the $^4$He molecular dimers that produce the original vacuum ultraviolet light. The prompt signal arises from the singlet dimers. De-excitation of triplet dimers takes a significantly longer time, leading to after-pulses. Triplet de-excitation is enhanced by mutual interaction (Penning ionization) that favors more rapid after-pulsing for highly ionizing particles where the energy is more densely deposited. The detection of the number of these single photoelectron events in the first few microseconds following the prompt pulse has been demonstrated in our R&D program (Hahn-Meitner) to provide adequate particle ID. The technique works best if there are at least 40 photoelectrons per event in the prompt signal.

A number of strategies, involving light detection at lower temperatures are being pursued to increase the number of photoelectrons detected. McKinsey [lxxxvii] has reported good performance from specially prepared PMTs operated at 27 K in liquid neon. These tubes have a thin metallic layer on the photocathode to prevent charge buildup that occurs due to higher photocathode resistivity at low temperatures. Because room temperature helium quickly destroys a PMT by diffusing through the glass, the PMTs must be located in vacuum rather than in the LHe space. If PMTs can be made to work at 4 K,

it will remove several of the gaps in the light guides necessitated by the heat load considerations and increase the number of photoelectrons significantly. Another possibility is to use visible-light photon counters (VLPC) with cryogenically cooled electronics instead of PMTs. VLPCs have much better quantum efficiency and are viable if they have sufficiently low dark current for individual photon counting in our environment. Laser fluorescence can also be used to measure the number of triplet states remaining after a fixed time following the prompt pulse [McKinsey]. This technique is under development and will be described in the R&D section of the CDR.

## A.2.f Magnetic fields and shielding {Caltech, Arizona State}

### Magnets

The nEDM measurement requires a static magnetic field surrounding the two target cells that contain the superfluid $^4$He, the polarized neutrons and the polarized $^3$He atoms. The applied static magnetic field, $B_0$, is chosen to be about 10 mG resulting in a precession of the magnetic moments for both neutrons and $^3$He nuclei of $\nu_i \sim 30$ Hz. To maintain the polarization of the neutrons and $^3$He atoms, the magnetic field should be uniform to 0.05% averaged over each cell volume with a time stability of one part in $10^7$ over the period of the precession. A separate requirement on the volume-averaged magnetic field gradient in the direction of $B_0$ of $\langle \partial B_x / \partial x \rangle < 0.01$ μG/cm is necessary to minimize the false EDM signal induced by motional $\vec{B} = \vec{v} \times \vec{E}$ effects. In addition, to reduce the influence of ambient external fields an overall magnetic-shielding factor of ~ $10^5$ is required. The basis for these requirements is summarized in Section C.2 and analyzed in more detail in the systematic-error discussion in Appendix XX (mag and mag shielding)

The current design for the target volume is shown in Figure 0.E. Here a single HV electrode is flanked by two parallel ground plates that provide equal and opposite electric fields over the two cell volumes. The static magnetic field is generated by a saddle-shaped cosθ coil, which gives an iron-free configuration with a sufficiently uniform $B_0$ magnetic field.

The design also includes a cylindrical ferromagnetic shield just outside of the $B_0$ coil to improve field uniformity, and a cylindrical superconducting shield to exclude external fields[1]. Interior to the $B_0$ coil are two additional coils that provide the oscillating $B_d$ field to achieve the dressed spin configuration of the experiment (discussed in Appendix XX). The geometry of all of these coils and shields are listed in Table 0-1. Additional coils (not shown in the figure) include a $\pi/2$ spin-flip coil to rotate the neutron and $^3$He spins by 90$^o$ and several gradient coils to provide well-defined magnetic field gradients in specific directions to study various systematic effects as discussed in Appendix XX. The feasibility of incorporating some of these coils into the structures of the $B_0$ and $B_d$ coils is under exploration. Smaller coils will provide the holding fields for the polarized $^3$He collection volume (also including a ferromagnetic shield to improve uniformity) and along the path to the measurement cell (see below) {Arizona State}.

[1] The ferromagnetic shield also reduces the effect of possible trapped flux in the superconducting shield that surrounds it.

| Component | Radius, *R* (m) | Length, L (m) |
|---|---|---|
| Inner Dressing Coil | 0.50 | 4.16 |
| Outer Dressing Coil | 0.59 | 4.16 |
| $B_0 \cos\theta$ Magnet | 0.65 | 4.16 |
| 4K Ferromagnetic Shield | 0.67 | 4.16 |
| Superconducting Shield | 0.69 | 4.16 |

**Table 0-1** Dimensions of the magnetic coils and low temperature magnetic shielding.

A preliminary design of the primary coil, the $B_0 \cos\theta$ magnet, has been completed based on analytic and finite element magnetic field calculations. We have optimized the field from a $\cos\theta$ saddle coil to provide a uniformity < 0.1 % while simultaneously providing a longitudinal gradient $\langle \partial B_x / \partial x \rangle < 0.01$ μG/cm. For $L/R$ = 6.4 and $N$ = 34 turns, we obtain a worst-case uniformity of 0.05% with a longitudinal gradient $\langle \partial B_x / \partial x \rangle = 0.007$ μG/cm. The uniformity goals for the static $B_0$ fields adopted for this nEDM experiment have thus been demonstrated to be attainable. Although this design is expected to be further optimized, this study provides an existence proof that the design goals can be met.

## Magnetic shielding

The experimental apparatus is enclosed within a 4-layer conventional magnetic shield ($\mu$-metal) designed to shield the experiment from the Earth's magnetic field and other (possibly time-varying) background fields. A schematic diagram of the 4-layer structure is shown in Figure 0.A. The material thickness for each layer has been chosen to be 0.062".

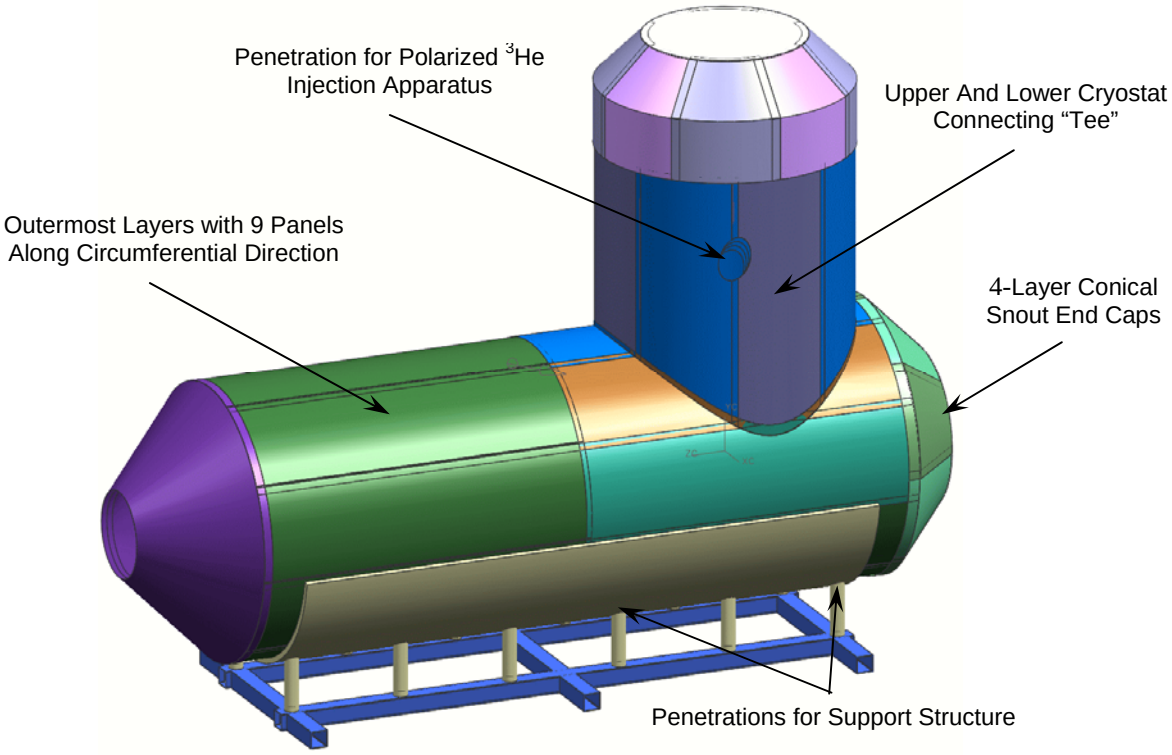


**Figure 0.A** The four layer conventional magnetic shielding structure.

A support structure (fabricated from aluminum) integrated with the support structures for the lower and upper cryostats is required to minimize stress on the $\mu$-metal panels, as stress or strain on the material will degrade its shielding performance. Cylindrical aluminum or other nonmagnetic material spacers will fill the regions between the layers and will be fabricated in a modular fashion similar to that for the $\mu$-metal panels.

The shield and the support structure will be designed so they can be assembled in a modular fashion. For example, the lower cryostat shielding surrounding the measurement cells may be assembled and installed before the rest of the shielding. Following installation of the lower cryostat and magnet infrastructure, the rear portion of the lower cryostat shielding, the connecting "tee", and the shielding for the upper cryostat may be installed as separate pieces. The design will also have to accommodate the need to remove the rear end-caps in a safe manner to provide access to the lower cryostat and measurement cell regions when necessary. Finally, battens tightened with aluminum screws and/or clamps will be used to provide overlapping magnetic seals across the seam lines between the many panels. An active degaussing system will also be incorporated into this system to maximize the shielding factor following re-assembly or exposure to significant external magnetic fields.

Preliminary estimates of shielding factors for the lower cryostat and upper cryostat shielding have been carried out with analytic and FEA (TOSCA) techniques. These calculations considered the shielding for the lower and upper cryostats separately, and ignored the presence of the superconducting shield, the connecting "tee", the end-caps, and all penetrations. The transverse shielding factors estimated by both techniques are on the order of a few $\times 10^5$. In the future, a full-model of the shielding structure (i.e., end-caps, penetrations, etc.) will be built within TOSCA.

## A.2.g $^3$He processing

The life cycle of the polarized $^3$He atoms in the EDM experiment consists of their production in an atomic beam source (ABS), injection into LHe and storage, transport into the measurement cell, eventual depolarization, and removal from the system. Most of these operations employ upper-cryostat equipment illustrated in Figure 0.A. More details are available in Appendix XX.

The ABS is a quadrupole filter that focuses one polarization and defocuses the other one. $^3$He atoms effuse into the filter from a 1 K volume of L$^3$He through a nozzle aimed along the axis of the filter. Large vacuum pumps remove the unwanted polarization state. The performance of this source (already constructed and tested) is measured to be $10^{14}$ atoms/s with 99.6% polarization. This flux allows the desired concentration to be accumulated in about 300 s.

The main LHe volume of the experiment, including the LHe in the measurement cells must have a very low concentration of unpolarized $^3$He - about $1\text{x}10^{-12}$ to maintain the overall neutron lifetime at ~ 500 s. This 'ultra-pure' LHe in the measurement cells (and extending into the $^3$He processing system - see below) is produced initially in a separate apparatus using McClintock's heat flush technique [lxxxviii][2]. Polarized $^3$He is injected into the system using the ABS to bring the concentration in the measurement cells to $1\text{x}10^{-10}$. The ABS is tilted at 45° to inject the beam into the collection volume - a ~ 1 l volume at ~ 0.5 K linked to the measurement cell and purification volumes as discussed below (see also Figure 0.B). . The exit of the ABS is designed so the trajectory of the $^3$He atoms does not intersect any walls before it intersects the LHe surface. The temperature of the injection volume must be low enough that the $^4$He vapor does not significantly impede the path of the polarized $^3$He atoms into the liquid. For the

[2] One of the purifiers built by McClintock has been acquired and operated by LANL.

saturated vapor at T = 0.5 K (p ~ $10^{-5}$ T) , the mean free path of He is ~ 2.5 cm and increases rapidly as the temperature decreases (e.g. 100 cm at 0.4 K). A magnetic-guide field maintains the polarization along the path. This field is tapered to provide adiabatic transport of the polarized atoms from the high field region of the source into the 10 mG holding field surrounding the collection volume.

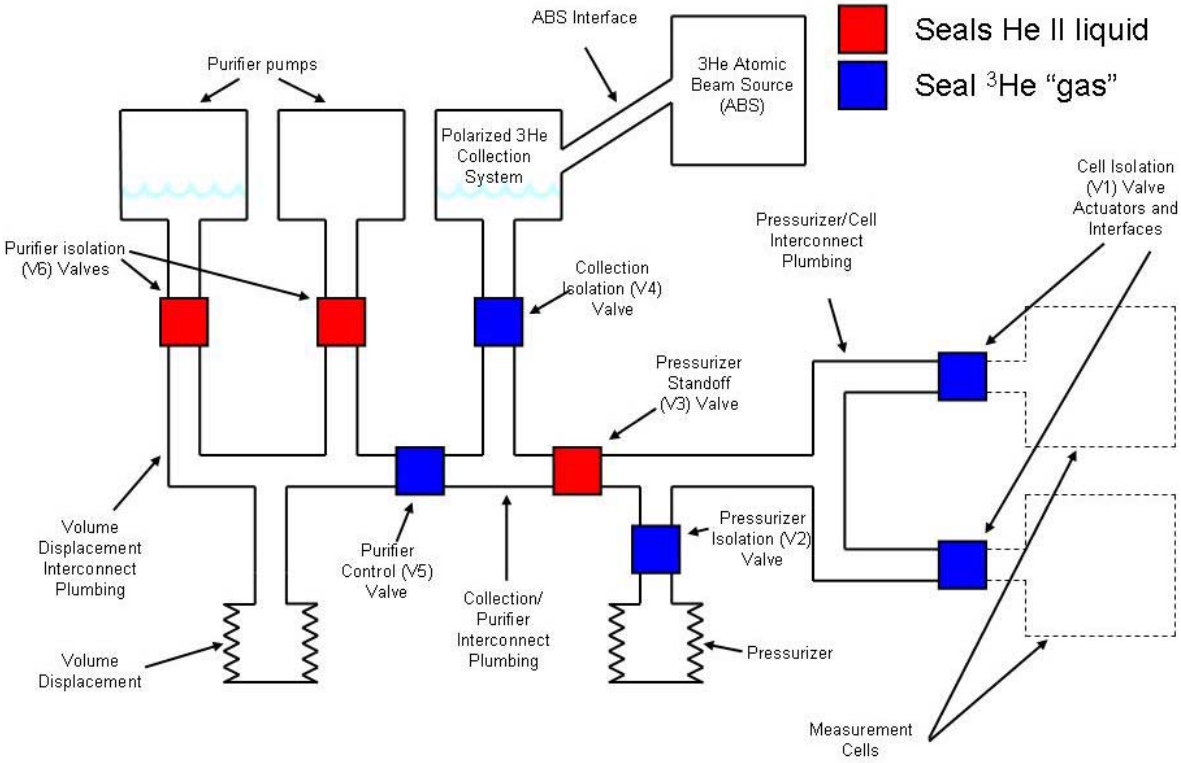


**Figure 0.B** Schematic layout of the $^3$He processing system. In a possible design of the purifier, two sorbtion pumps are used; the pump on the right can be regenerated in the configuration shown above. A possible pressurizer (potentially used to increase the dielectric strength of the LHe) is also shown schematically.

The fields and materials in the $^3$He processing system, and especially in the region of the measurement cells where the $^3$He spends most of its time, must all be compatible with maintaining the polarization of the atoms to the extent possible. At this stage, it appears that plastics such as acrylic are likely to afford the longest relaxation times and be consistent with the many other requirements (including low neutron activation probability and relatively benign products). Processing of these materials for the valves and 'plumbing' will all necessarily be custom, with special attention to, for example, the differential thermal contraction at plastic to metal and plastic to glass joints.

Motion of the $^3$He in the system (roughly speaking from the collection volume to the measurement cells and from the measurement cells to a purifier) will be effected in one of two ways. In the simplest implementation, because the diffusion constant of $^3$He in LHe ~ $T^{-7}$ [Lamoreaux], its motion is ballistic in our system below about 0.35 K, i.e. one can think of the LHe as a vacuum from the point of view of the $^3$He (~ a very low pressure gas). If the experiment could be operated at this temperature, we could rely on this 'molecular' flow to move the $^3$He around the system with the addition of a few valves and a purifier (see below).

However, because of the potential effects of the so-called geometric phase systematic error related to magnetic field gradients (see Systematic Uncertainty section below), the diffusion constant cannot be increased without bound. Although the final optimization of temperature (diffusion constant) has not

been completed, we are planning for the possibility of using a small temperature gradient within the system to take advantage of the heat flush effect to move the $^3$He from place to place. For $T < T_\lambda$, a temperature gradient in LHe generates a so-called thermomechanical effect. In the two-fluid model, it is the normal fluid that must carry the energy (as phonons for T< 0.6 K) and the $^3$He is effectively swept along with it (the superfluid moves in the opposite direction such that the overall density remains constant). In combination with the system of valves in Figure 0.B, ordering the temperatures of the collection volume, measurement cell and purifier ($T_{cv} > T_{mc} > T_p$) can produce the desired transport. To be specific, we calculate that temperature gradients of about 40 mK on either side of a measurement cell temperature of 0.4 K, can produce the desired effect in times of order 100 s and for heat inputs of a few mW (well within the capacity of the refrigeration). The results from a simulation at a slightly lower temperature (worse case) are shown in Figure 0.C.

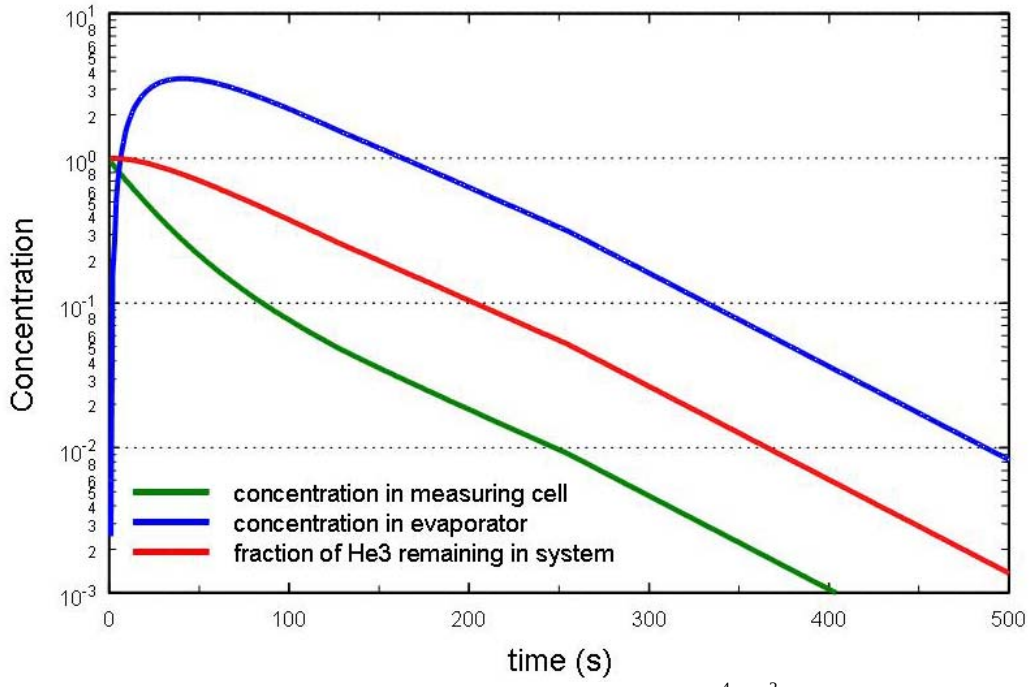


**Figure 0.C** Example of heat flush technique. Measurement cell at 0.35 K ($10^4$ cm$^3$ volume), purifier (200 cm$^2$ free surface area, 500 cm$^3$ volume) at 0.31 K; interconnecting tube 3.5 cm diameter, 200 cm long; heat flow 4.5 mW.

Purification of the LHe might be done in either of two ways. Because the binding energy of $^3$He in LHe is less than that of $^4$He (3 K vs. 7 K), pumping the vapor over an open surface of LHe at a temperature of about 0.36 K can result in a two order of magnitude reduction in the $^3$He in of order 100 s. In this case, the pump would be a standard activated charcoal sorption device (including an appropriate film burner to prevent the superfluid from wetting the absorber). If we need to run the 'purifier' at a lower temperature, we could simply rely on the heat flush to sequester the high concentration $^3$He liquid in a valved-off volume with makeup LHe provided from a pure reservoir (and periodically replenished by LHe purified by the McClintock purifier).

Most of the valves in the system are required simply to limit the transport of $^3$He to places where it might be depolarized more easily (and then diffuse back into the system). In the event that we need to pressurize the LHe to provide a high dielectric strength, one or more valves will be required to be superfluid tight with a pressure difference of ~ 1 atm across them. This is the most stringent requirement; we have successfully prototyped a "cork in bottle" style valve stem and seat that is superfluid tight at the leak rate limit of a standard leak detector ($10^{-9}$ std cm$^3$/s). The stem and seat are 1 in. in diameter and

made from Vespel (a plastic which is a bulk form of the more familiar kapton film). To date, we have been successful in testing a leak tight valve prototype with approximately 200 closures (completed with the valve operating normally) to a sealing force of about 80 pounds and with a pressure difference across the valve of ~ 0.5 atm (limit of present pressurizing apparatus). We plan to extend the reliability tests and increase the pressure difference across the valve in a new apparatus where a complete valve assembly (including a prototype actuator which has an appropriately small heat load) can be tested.

### A.2.h Refrigeration

The optimal operating temperatures are expected to lie between 0.3 - 0.5K. Three refrigerators will be used to maintain the system at the operating point. The cool down from 4 K to below $T_\lambda$ is managed by a pumped $^4$He refrigerator. Two dilution refrigerators (DRs) are used for the remaining cooldown and for steady state operation. Roughly, one can think of each DR being associated with each of the upper and lower cryostats. One such DR has been purchased and operated by LANL from Leiden and provides ~ 80 mW at 0.5 K; the experiment is designed to operate at roughly 2/3 the capacity of the refrigerators. Further details and the heat budget for the experiment may be found in Appendix XX (http://www.npl.uiuc.edu/exp/nEDM/NSFAppendices).

### A.2.i Data acquisition and slow controls

The signals in the experiment consist of scintillation light pulses collected and detected with a more or less conventional system of light guides and PMTs. Data will be collected in two parallel streams. A standard discriminator/scaler system will be used for on-line diagnostics and control. Because of the possibility of performing additional particle i.d. based on LHe scintillation after-pulses from heavily ionizing particles, data will also be collected with coincidence-triggered wave form digitizers. Data-collection from the SQUIDS must be performed concurrently. With an event size of about 10 kB and an event rate on the order of 1 kHz, over the course of a year (30% live time) this amounts to ~100 TB indicating the clear need for data-reduction in the analysis process.

The operation of the experiment requires an extensive slow controls system involving of order 1000 I/O points. Our controls will be based on the standard EPICS (the standard at many accelerator laboratories including SNS). During a single standard measurement period, an involved sequence of steps are required from neutron and $^3$He collection, to control of E and B fields, to data acquisition, to $^3$He purification. We anticipate a number of similar, but special, sequences for diagnostic purposes. In addition, there are many temperatures, pressures, etc. for the apparatus that must be monitored and, in many cases, controlled. Because EPICS is an inherently distributed system, we anticipate building up the slow controls for individual subsystems as they are developed, to be available for the sequence of subsystem testing.

### A.2.j Measurement cycle

Table II-1 is a summary list of the steps in a measurement cycle along with illustrative durations. The durations remain to be optimized to achieve maximal sensitivity once the UCN storage and $^3$He relaxation times are known. The table assumes that the starting condition is that the upper and lower cryostats are free of both UCN and $^3$He.

**Table II-1. The Steps in an EDM Measurement Cycle.**

| Step | Description | Duration (s) |
|---|---|---|
| 1 | Polarized $^3$He atoms move into the measurement cell (diffusion or heat flush) | 100 |
| 2 | Illuminate the measurement cell with polarized cold neutrons to produce polarized UCN aligned with the $^3$He atoms | 1000 |
| 3 | Apply $\pi/2$ pulse to rotate spins to be perpendicular to the magnetic field | 10 |

| | | |
|---|---|---|
| 4 | Measure precession frequency | 500 |
| 5 | Remove $^3$He atoms from system | 100 |
| 6 | Reload the collection volume with polarized $^3$He from the ABS | 300 |
| 7 | Return to step 1 | N/A |

## A.3 Expected Sensitivity and Systematic Effects

### A.3.a Scintillation signal sensitivity

The EDM pre-proposal develops the arguments for the sensitivity of this experiment under certain assumptions [lxxxix, p. 140]. Those assumptions include:

(1) The backgrounds to the scintillation measurement are roughly 1:1 with the signal and have an exponential decay spectrum with a decay constant close to that of the bottle storage time.

(2) The polarizations in the problem are P($^3$He) ≡ $P_3 \cong 1$, P(cold neutrons) ≡ $P_{cn} \cong 0.9$, and the P(UCN) ≡ $P_n \cong 0.96$. $P_n$ exceeds $P_{cn}$ because the polarized $^3$He is preferentially absorbing the "wrong" spins-state neutrons during the filling process.

(3) The number of neutrons in the two cells combined is 0.86 $PV\tau$, where $P$ is the combined UCN production rate, $V$ is the volume of one cell (4000 cm$^3$) and $\tau$ is the neutron lifetime in the apparatus, including $^3$He absorption, beta decay, and wall losses, taken to be equal to the natural lifetime of the neutron or about 1000 s.

For the nominal SNS production rate of 0.3/cm$^3$/s, the sensitivity to a frequency shift due to the electric field is 4.7 μHz per cycle, which translates to a $1\sigma$ sensitivity for the EDM of

$$9.3\times10^{-27} e\cdot\text{cm}\sqrt{\frac{\text{days}}{T}} \qquad \text{(II.5)}$$

with $T$ defined as the total live time of the experiment in days. This project intends to collect data for 300 live days over three calendar years, leading to a $1\sigma$-sensitivity of

$$5.4 \times 10^{-28}\ e\cdot\text{cm}. \qquad \text{(II.6)}$$

Two factors may modify the result in Equation II.6. Particle ID can greatly reduce the background assumption (1) above. If the background is essentially eliminated, there is a factor-of-two improvement in the sensitivity [xc]. In a background-free experiment, the measurement time should be extended relative the UCN filling time taken as equal in Equation II.5. This optimization should lead to another factor-of-two improvement [xc]. Putting in these factors, the $1\sigma$ sensitivity becomes

$$1.4 \times 10^{-28}\ e\cdot\text{cm}. \qquad \text{(II.7)}$$

### A.3.b SQUID magnetometer sensitivity

It is necessary to use the $^3$He precession signal to determine the average magnetic field affecting the UCN precession. Ideally, the field would be constant; however, there are potential changes due to finite shielding of ambient magnetic field changes, and fields due to leakage currents associated with the application of HV.

Because the $^3$He and neutron magnetic moments are equal to within 10% and because the electric field does not affect the $^3$He precession, it is only the difference in magnetic Larmor precession frequencies that needs to be known to high accuracy. The ultimate sensitivity per measurement cycle is 0.65 μHz (corresponding to Equation II-7), so the minimum required accuracy on $\delta B$ is

$$\delta B = \frac{1.2\mu\text{Hz}}{|\gamma_3 - \gamma_n|} = 370\ \text{fT} \qquad \text{(II.8)}$$

per measurement cycle; practically, the accuracy on $\delta B$ should be a factor of three smaller so that it does not contribute noise to the measurements.

The noise in a SQUID system has been analyzed in the preproposal [lxxxix, p. 143], and the condition in Equation II.8 translates into a noise criteria of

$$0.18\mu\Phi_0 / \sqrt{\text{Hz}} / \text{cm}^2 . \quad \text{(II.9)}$$

The commercial Conductus-1020 SQUID has a noise level of $3\mu\phi_0/\sqrt{Hz}$, implying that a ~ 16 cm$^2$ pickup loop is required to attain the required signal-to-noise ratio. This noise level is consistent with the extrapolation of a recent test using SQUID detection for an NMR measurement of a room temperature polarized $^3$He sample. Note that the above calculation assumes the $^3$He polarization does not decay significantly over the measurement period. In any case, care must be taken in the experiment to reduce the external sources of noise, as well as to adequately shield the SQUIDS and associated electronics.

**A.3.c Systematic effects**

This section addresses possible systematic effects that are "fundamental" as opposed to the usual concerns of external magnetic fields associated with reversing HV apparatus, etc. Of course, such effects can be important for the proposed experiment but will be largely suppressed by the internal $^3$He co-magnetometer. The issues discussed here lead to real differences in the effective magnetic field seen by the $^3$He and UCN and have been described in more detail in the preproposal [lxxxix, p. 144].

*A.3.c.1 Pseudo-magnetic Field*

The effective UCN potential is given in terms of the coherent scattering length of each spin state of every constituent in the measuring cell. In the case where the constituents are polarized, each spin state has a different potential; this energy difference creates a pseudo-magnetic field. For polarized $^3$He at a fractional concentration of $10^{-10}$, the difference in the scattering lengths leads to a raw frequency shift of 660 μHz when the $^3$He polarization lies along the static magnetic field. This large shift is reduced by a number of factors as follows.

First, this shift is not dependent on the electric field, so it is canceled by the two cells having opposite electric fields. , but can introduce noise into the system if it varies between the two cells between fillings.

First, the $^3$He spins are flipped into the plane for the free precession measurement, so the average field seen by the UCN has near-zero average; the only contribution to the precession frequency is that due to the imprecision of the π/2 pulse. Achieving 5% accuracy for this pulse reduces the pseudo-magntic precession to 33 μHz. Furthermore, the cells are filled with almost exactly the same $^3$He density because both are filled from the same source, so the difference frequency is even smaller. The initial $^3$He density is expected to be the same within 5%. Furthermore, the relative difference in the π/2 pulse between cells can be accurate to within 1%. These various factors bring the pseudo-magnetic precession frequency difference to less than 1 μHz, which is sufficiently below the initial expected accuracy of about 2.6 μHz per measurement cycle so that no extra noise will be introduced. However, the importance of comparing two cells filled from the same source is evident. The direct $^3$He magnetic field and its effect on the UCN is too small to be of concern compared to the pseudo-magnetic field.

*A.3.c.2 Gravitational offset and other spatial UCN/$^3$He differences*

The density of UCNs "sags" under the influence of the Earth's gravitational field because their kinetic energy is so low. The shift in center of mass of UCN in a storage chamber of height $h$ was estimated in Reference [lxxx], p. 93

$$\Delta h = \frac{mgh^2}{3kT}. \quad \text{(II.10)}$$

For $h$ = 10 cm and $T$ = 3 mK, $\Delta h$ = 0.13 cm. The $^3$He energy (effective temperature) is ~ 0.4 K compared to 3 mK for the UCN, so the effect of gravity on the $^3$He distribution is extremely small. The principal concern is that, if there is a spurious field from leakage currents, the $^3$He and UCN will not average it in the same way. The problem cannot be solved exactly because the leakage current distribution is unknown, but the effect can be estimated. The usual rule of thumb is that the current is assumed to flow in a ¼-turn loop around the cell. Assuming a current of 1 nA, which is likely achievable at low temperature, and the average displacement of the two species, the maximum systematic error of $10^{-29}$ $e$·cm is comfortably below the anticipated statistical limit.

A related concern is nonuniformity of the $^3$He distribution due to wall interaction. The effort to detect a nonuniformity in the $^3$He distribution in a test cell (by use of neutron tomography [Hayden]) shows no substantial effects. In fact, it is anticipated that the $^3$He will be repelled by the superfluid/cell interface. Unlike the case of most atoms that experience a Van der Waals attraction, or even near chemical binding, to walls of storage cells, the case of $^3$He in superfluid helium is special (consistent with the rapidly increasing relaxation times observed by Himbert and Dupont-Roc as the superfluid film condenses on the cell walls [Himbert]).

*A.3.c.3 Motional magnetic field effects*

The motional, or $\vec{v} \times \vec{E}$, magnetic field introduces a problem because the UCN and $^3$He atoms have very different average velocities (although the effective diffusive velocity of $^3$He at the higher temperatures is similar to that of the UCNs). However, the motional field is randomly fluctuating because the velocity changes on subsequent collisions with the cell walls. The problem is discussed in Reference [xci], Section 3.5.3, and in Reference [xcii], where it is shown that the effect is "quadratic" in that it is proportional to the square of the electric field. The conclusion is that, for a 50 kV/cm field, the electric field must reverse with an accuracy of 1% to maintain a systematic shift below $5 \times 10^{-29}$ $e$·cm. The electric field reversal accuracy is easily met and checked with the Kerr-effect measurement.

*A.3.c.4 Geometric phase effect*

The geometric phase effect arises from the motion of, e.g. a polarized $^3$He atom or UCN, in a plane perpendicular to the holding field direction (referred to as its 'orbital' motion below). In the particle rest frame, the overall magnetic field vector (holding field and any radial field) appears to precess around the particle spin direction, generating a 'geometric phase' and a corresponding frequency shift [LamoreauxGolub, Commins]. In the nEDM experiment, the difficulty arises because the magnitude of the radial field has contributions both from a gradient in the holding field (via Maxwell's Equations) and from the $\vec{v} \times \vec{E}$ motional field (see Figure 0.A). This contribution to the particle's precession frequency is linear in $\vec{E}$. Further, if the particle's orbital frequency is much larger (smaller) than the Larmor frequency, the contribution is independent of (quadratic in) the orbital frequency (in the latter case one power of the orbital frequency from the motional field, and one because the geometric phase arises in the particle, i.e. rotating, frame).

The recent discussion of the effect began in the context of the cylindrical geometry of the newly completed ILL EDM experiment [[xciii]]. In this case, the orbital frequency is much larger than the Larmor frequency and

$$\delta\omega = \frac{\gamma^2 \frac{\partial B}{\partial R} R^2 E}{c}, \qquad \text{(II.11)}$$

a frequency shift that is only somewhat smaller than the reported upper limit. For both experiments, the geometric phase effect for the UCNs is quadratic in the orbital frequency and small. For the present experiment, the situation for $^3$He is intermediate between the two extremes, depending on the $^3$He auto-

correlation function (and does not cancel the neutron effect). The effect does cancel between the two cells to first order if the nonuniformity is symmetric about $x = 0$ (center of the HV electrode). For a 10 mG holding field, the nonuniformity across the cell needs to be 0.1 μG to minimize the effect on the sensitivity, a quite challenging requirement. Because the time between collisions for $^3$He varies with temperature due to the rapidly varying diffusion coefficient, the effect is quite temperature dependent. In order to maintain the geometric phase effect safely below the ultimate sensitivity, measurement and simulation of magnetic field uniformity suggests that the cell temperature should be at or about 0.4 K.

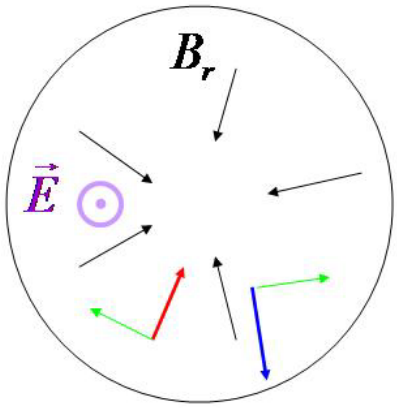


**Figure 0.A** The geometric phase effect effectively involves an 'interference' between the radial magnetic field (arising from a gradient in the holding field) and the motional electric field. In this interference, changing the direction of the velocity vector (green), changes the direction of $\vec{v} \times \vec{E}$ (red and blue), but not the frequency shift.

## B. References


i. J. Chadwick, *Nature* **129**, 312 (1932);
*Proc. Roy. Soc.* (London) **A136**, 692 (1932).
ii. E.M. Purcell and N.F. Ramsey, *Phys. Rev*. **78**, 807 (1950).
iii. J.H. Smith, E.M. Purcell, and N.F. Ramsey, *Phys. Rev*. **108**, 120 (1957).
iv. C.A. Baker et al., (submitted to *Phys. Rev. Lett*.) [http://arxiv.org/abs/hep-ex/0602020].
v. A. Angelopoulos et al. (CPLEAR Collaboration), *Phys. Lett*. **444B**, 43 (1998).
vi. G. Buchalla et al., *Nucl. Phys*. **B370**, 69 (1992);
A.J. Buras et al., *Nucl. Phys*. **B408**, 209 (1993);
M. Ciuchini, *Nucl. Phys. Proc. Suppl*. **59**, 149 (1997).
vii. R. Tribble, chair. Subcommittee on Fundamental Physics with Neutrons Report to the Nuclear Science Advisory Committee (2003) [http://www.sc.doe.gov/production/henp/np/nsac/nsac.html].
viii. S. Weinberg, *The First Three Minutes* (Harper-Collins Publishers, NY, 1977), p.95.
ix. A.D. Sakharov, *JETP Lett.* **5**, 24 (1967).
x. V.A. Kuzmin, V.A. Rubakov, and M.E. Shaposhnikov, *Phys. Lett.* **155B**, 36 (1985).
xi. M. Fukugita and T. Yanagita, *Phys. Lett*. **174B**, 45 (1986).
xii. M.E. Shaposhnikov, *Nucl. Phys. B* **287**, 757 (1987).
xiii. G. 't Hooft, *Phys. Rev. Lett*. **37**, 8 (1976).
xiv. A.G. Cohen, D.B. Kaplan, and A.E. Nelson, *Annu. Rev. Nucl. Part. Sci*. **43**, 27 (1993).
xv. K. Kajantie et al., *Nucl. Phys. B* **466**, 189 (1996).
xvi. A. Riotto, *Phys. Rev. D* **58**, 095009 (1998).
xvii. M. Carena, et al, *Nucl. Phys. B* **503**, 387 (1997);
M. Carena et al, *Nucl. Phys. B* **599**, 158 (2001).
xviii. C. Balazs, M. Carena, and C.E.M. Wagner, *Phys. Rev. D* **70**, 015007 (2004).

xix. C. Lee, V. Cirigliano, and M.J. Ramsey-Musolf, *Phys. Rev. D* **71**, 075010 (2005).
xx. C. Balazs, et al, *Phys. Rev. D* **71**, 075002 (2005).
xxi. V. Cirigliano et al., (to be published in Phys. Rev. D) [http://arxiv.org/abs/hep-ex/0603058].
xxii. T. Konstandin, T. Prokopec, and M.G. Schmidt, *Nucl. Phys. B* **716**, 373 (2005);
*Nucl. Phys. B* **679**, 246 (2004).
xxiii. T. Konstandin et al, [http://arxiv.org/abs/hep-ex/0505103].
xxiv. V. Cirigliano et al., [http://arxiv.org/abs/hep-ex/0603246].
xxv. V. Baluni, *Phys. Rev. D* **19**, 2227 (1979).
xxvi. R.J. Crewther et al., *Phys. Lett*. **88B**, 123 (1979);
Errata, **91B**, 487 (1980).
xxvii. I.I. Bigi and A.I. Sanda, *CP Violation* (Cambridge University Press, Cambridge, UK, 2000).
xxviii. R. Peccei and H. Quinn, *Phys. Rev. Lett*. **38**, 1440 (1977);
*Phys. Rev. D* **16**, 1791 (1977).
xxix. S. Barr and A. Zee, *Phys. Rev. Lett.* **55**, 2253 (1985).
xxx. I.B. Khriplovich and A.R. Zhitnitsky, *Phys. Lett.* **109B**, 490 (1982).
xxxi. M.B. Gavela et al., *Phys. Lett.* **109B**, 215 (1982);
B. McKellar et al., *Phys. Lett B* **197**, 556 (1987).
xxxii. M.E. Pospelov and I.B. Khriplovich, *Yad. Fiz*. **53**, 1030 (1991*)* [*Sov. J. Nucl. Phys*. **53**, 638 (1991)].
xxxiii. see B. Aubert, [http://arxiv.org/abs/hep-ex/0203007] and
K. Abe, [http://arxiv.org/abs/hep-ex/0202027] and
references therein.
xxxiv. W. Bernreuther and M. Suzuki, *Rev. Mod. Phys*. **63**, 313 (1991).
xxxv. Yale Proposal. De Mille, Search for an Electron Electric Dipole Moment in the *a*(1) state of Pb0.
[xxxvi]. S.K. Lamoreaux, *Phys. Rev. A* **66**, 022109 (2002);
B.J. Heidenreich et al., *Phys. Rev. Lett*. **94**, 253004 (2005).
[xxxvii]. J. Dobaczewski and J. Engel, *Phys. Rev. Lett.* **94**, 232502 (2005).
xxxviii. R.N. Mohapatra, *Unification and Supersymmetry*, (Springer-Verlag, 1992).
xxxix. P. Herczeg, in *Symmetries and Fundamental Interactions in Nuclei*, ed. W. C. Haxton and E. Henley
(World Scientific, 1995).
xl. G. Beall and N.G. Deshpande, *Phys. Lett*. **132B**, 427 (1983).
xli. D. Chang, W.-Y. Keung, and T.C. Yuan, *Phys. Lett*. **251**, 608 (1990).
xlii. I.I. Bigi and N.G. Uraltsev, *Nucl. Phys. B* **353**, 321 (1991).
xliii. M.S. Barr and A. Zee. *Phys. Rev. Lett.* **65**, 21 (1990).
xliv. J. Gunion and D. Wyler, *Phys. Lett*. **248B**, 170 (1990).
xlv. R.G. Leigh, S. Paban, and R.-M. Xu, *Nucl. Phys. B* **352**,45 (1991).
xlvi. C. Bowser-Chao, D. Chang, and W.-Y. Keung, *Phys. Rev. Lett*. **79**, 1988 (1997).
xlvii. S.M. Barr, *Int. Journal Mod. Phys. A* **8**, 209 (1993).
xlviii. R. Barbieri, A. Romanino, and A. Strumia, *Phys. Lett.* **369B**, 283 (1996).
[xlix]. M. Pospelov and A. Ritz, *Ann. Phys.* **318**, 119 (2005).
l. T. Falk et al., *Nucl. Phys. B* **560**, 3 (1999).
li. J.P. Jacobs et al., *Phys. Rev. Lett*. **71**, 3782 (1993);
M. Romalis et al*., Phys Rev. Lett.* **86**, 2505 (2001).
lii. S. Dimopoulos and L.J. Hall, *Phys. Lett*. **344B**, 185 (1995).
liii. J.H. Smith, Ph.D. thesis, Harvard University, 1951 (unpublished).
liv. T.D. Lee and C.N. Yang, *Phys. Rev*. **104**, 254 (1956).
lv. N.F. Ramsey, *Molecular Beams* (Oxford University Press, Oxford, 1956).
lvi. C.S. Wu et al., *Phys. Rev.* **105**, 1413 (1957).
lvii. R. Garwin, L. Lederman, and M. Weinrich, *Phys. Rev*. **105**, 1415 (1957).
lviii. J. Friedman and V. Telegdi, *Phys. Rev*. **105**, 1681 (1957).
lix. L. Landau, *Nucl. Phys*. **3**, 127 (1957).
lx. I.B. Zel'dovich, *J. Exp. Theor. Phys*. **6**, 1488 (1957) [*Sov*. *Phys. JETP* **6**, 1148 (1957)].
lxi. N.F. Ramsey, *Phys. Rev.* **109**, 222 (1958).
lxii. J. Schwinger, *Phys. Rev.* **82**, 914 (1951);
**91**, 713 (1953).

lxiii. G. Lüders, *Kgl. Danske Videnskab Selskab. Mat. Fiz. Medd*. **28**, No. 5 (1954);
G. Lüders and B. Zumino, *Phys. Rev.* **106**, 385 (1957).
lxiv. W. Pauli, in *Niels Bohr and the Development of Physics* (McGraw-Hill, New York, 1955).
lxv. J.H. Christenson et al., *Phys. Rev. Lett.* **13**, 138 (1964).
[lxvi]. http://minoserv.maps.susx.ac.uk/~nedm/indexhtm.
[lxvii]. N.F. Ramsey, *Phys. Rev.* **76**, 996 (1949).
[lxviii]. http://ucn.web.psi.ch/.
[lxix]. http://physics.valpo.edu/facultyResearch/proposal_MDM/
lxx. M.V. Romalis et al., *Phys. Rev. Lett*. **86**, 2505 (2001).
lxxi. T.G. Vold et al., *Phys. Rev . Lett*. **52**, 2229 (1984).
lxxii. http://www.atomic.princeton.edu/romalis/CP/.
lxxiii. http://www-mep.phy.anl.gov/atta/research/radiumedm.html.
lxxiv. E.D. Commins et al., *Phys. Rev*. *A* **50**, 2960 (1994).
[lxxv]. J.J. Hudson et al., *Phys. Rev. Lett.* **89**, 023003 (2002).
[lxxvi]. http://pantheon.yale.edu/%7Edpd5/EDM.htm.
[lxxvii]. S.K. Lamoreaux, *Phys. Rev. A* **66**, 022109 (2002).
[lxxviii]. Y.K. Semertzidis et al., In the proceedings of KEK International Workshop on High Intensity Muon Sources (HIMUS 99), Tsukuba, Japan, Dec 1999, (hep-ph/0012087).
[lxxix]. Y.K. Semertzidis et al. (EDM Collaboration), AIP Conf.Proc.**698**:200–204, 2004 [hep-ex/0308063].
lxxx. R. Golub and S.K. Lamoreaux, *Physics Reports* **237**, 1 (1994).
lxxxi. P. Ageron et al., *Phys Lett.* **A66**, 469 (1978);
R. Golub et al., *Z. Phys*.**B51**, 187 (1983);
R. Golub, *J. Phys*. **44**, L321 (1983);
Proc. 18th Int. Conf. on Low Temperature Physics, Pt. 3 Invited Papers (Kyoto, Japan), 2073 (1987);
R. Golub and S.K. Lamoreaux, *Phy. Rep*. **237**, 1 (1994);
R. Golub and J.M. Pendlebury, *Phys. Lett. A* **62**, 337 (1977).
lxxxii. S.K. Lamoreaux and R. Golub, *JETP Lett*. **58**, 793 (1993).
lxxxiii. S.K. Lamoreaux, Institut Laue-Langevin Internal Report 88LAOIT, 1988, unpublished;
J.M. Pendlebury, *Nuc. Phys*. **A546**, 359 (1992).
lxxxiv. P.R. Hoffman et al., *Nature* **403**, 62 (2000).
[lxxxv]. D.R. Rich, et al. *Nucl. Instrum. and Meth. A* **481**, 431 (2002);
O. Zimmer, et al. *EPJDirect* **A1**, 1 (2002);
C.D. Keith, et al. *Phys. Rev. C* **69**, 034005 (2004).
lxxxvi. C.A. Baker et al., (submitted to *Phys. Rev. Lett.*) [http://arxiv.org/abs/hep-ex/0602020].
Romalis M. V. Romalis, et al. *Phys. Rev. Lett.* **86** (2001) 2505.
Schiff L. I. Schiff, *Phys. Rev.* **132** (1963) 2194.
Budker Sushkov, A. O., et al., *Phys. Rev. Lett.* 93 (2004) 153003.
[lxxxvii]. J. A. Nikkel et. al., astro-ph/0702202
McKinsey D. N. McKinsey, et al. Phys.Rev.Lett. 95 (2005) 111101.
[lxxxviii]. P.V.E. McClintock, *Cryogenics* **18**, 201 (1978);
P.C. Hendry and P.V.E. McClintock, *Cryogenics* **27**, 131 (1987).
lxxxix. A New Search for the Neutron Electric Dipole Moment, Pre-proposal submitted to the Department of Energy, by the EDM Collaboration 2002.
[xc]. E. Van Cleve and M.D. Cooper, EDM Technical Note: Sensitivity of the Liquid He EDM Experiment as Derived from Least Squares Fitting of Pseudo-Data and Comparisons to the Heisenberg-Uncertainty Principle, LAUR-02-5924 (2002).
[Hayden] M. Hayden, et al. *Europhys. Lett.* **58** (2002) 718.
[Himbert] M. Himbert and J. Dupont-Roc. *J. Low Temp. Phys.* **76** (1989) 435.
xci. T.G. Vold et al., *Phys. Rev. Lett.* **52**, 2229 (1984).
xcii. S.K. Lamoreaux, *Phys. Rev. A* **53**, 3705 (1996).
[LamoreauxGolub] A. L. Barabanov, R. Golub and S. K. Lamoreaux, nucl-ex/0512014.
[Commins] E. Commins, *Am. J. Phys.* **59**, 1077 (1991).
[xciii]. J.M. Pendlebury et al. *Phys. Rev. A* **70**, 032102 (2004);
P.G. Harris and J.M. Pendlebury, *Phys. Rev. A* **73**, 014101 (2006).